Epsin2, a novel target for multiple system atrophy therapy via regulating α-synuclein propagation associated with FABP7

An Cheng[1, 2, *], Yifei Wang[1], Tomoki Sekimori[2], Wenbin Jia[1, 2], Yi Chen[3], David I Finkelstein[4], Ichiro Kawahata[2], Takuya Sasaki[1, *], Kohji Fukunaga[2,5, *]

[1] Department of Pharmacology, Graduate School of Pharmaceutical Sciences, Tohoku University, Sendai, Japan

[2] Department of CNS Drug Innovation, Graduate School of Pharmaceutical Sciences, Tohoku University, Sendai, Japan

[3] Department of Industrial Engineering & Decision Analytics, Hong Kong University of Science and Technology, Hong Kong

[4] Mental Health Research Institute, The University of Melbourne, Victoria, Australia

[5] Lead contact

* Correspondence should be addressed to An Cheng (leon.an.cheng.1q84@gmail.com); Takuya Sasaki (t.sasaki.0224@gmail.com); Kohji Fukunaga (koji.fukunaga.c1@tohoku.ac.jp)

SUMMARY

Background: Multiple system atrophy (MSA) is an adult-onset, fatal neurodegenerative disease featured by propagation of misfolded α-synuclein and dysregulation of myelin integrity in central nervous systems (CNS). In our previous study, we identified that fatty acid binding protein 7 (FABP7), one glial protein regulated α-synuclein (α-syn) toxicity and closely related to oligodendrocyte loss. Here, we investigated how FABP7 works in MSA pathological process.

Methods: The mouse model of MSA: PLP-hαSyn transgenic mice (PLP-hαSyn mice) were used for understanding the underling role of FABP7 in α-syn aggregation. *In vitro,* FABP7/α-syn hetero-aggregates were constructed by recombinant human-α-syn and 6X His-tag human-FABP7. By immunohistochemical analyze of brain tissue from PLP-hαSyn mice and aggregates injection mice, we identified the toxicity of aggregates and the region or cell type in brain which aggregates prefer to propagate. Furthermore, through the bioinformatics analysis of MSA patient blood, PLP mouse brain tissue we found candidate proteins related to α-syn propagation. Then, the hypothesis was verified by adeno-associated virus (AAV) knockdown in aggregates injection mice.

Findings: In PLP-hαSyn mice, FABP7 also forms hetero-aggregates with α-syn and the FABP7/α-syn hetero-aggregates exhibited higher molecular weight and stronger toxicity than α-syn aggregates both *in vitro* and *in vivo*. The same with PLP-hαSyn mice, in the FABP7/α-syn hetero-aggregates injected mice, aggregates prefer to accumulate in oligodendrocyte and purkinje neurons. By bioinformatics analysis we found the protein epsin-2 as a potential receptor which regulate FABP7/α-syn hetero-aggregates propagate to oligodendrocytes and purkinje neurons. In AAV-dependent epsin-2 knock down mice we observed decreased levels of FABP7/α-syn hetero-aggregates in purkinje neurons and oligodendrocytes.

Conclusions: These data suggest that epsin-2 is an important potential therapeutic target for MSA via regulating FABP7/α-syn hetero-aggregates propagation. It is very meaningful for further investigation and developing specific inhibitors.

Funding: This work was supported by the Strategic Research Program for Brain Sciences from the Japan Agency for Medical Research and Development (JP17dm0107071, JP18dm0107071, JP19dm0107071, and JP20dm0107071).

Keywords: Multiple system atrophy, FABP7, α-synuclein aggregates, epsin-2

INTRODUCTION

Multiple system atrophy (MSA) is an adult-onset, fatal neurodegenerative disease clinically characterized by progressive autonomic failure, parkinsonism, and cerebellar and pyramidal tract symptoms(Fanciulli and Wenning, 2015). The pathological hallmark of MSA is the abnormal accumulation of misfolded α-synuclein (α-syn), which contains 140 amino acids and expresses in the presynaptic terminals of neurons(Spillantini et al., 1997) in glia cells, called glial cytoplasmic inclusions (GCI). Therefore, MSA is also classified as an oligodendroglia α-synucleinopathy like Parkinson's disease (PD), dementia with Lewy bodies disease (DLBD)(Spillantini et al., 1998). However, different form PD or DLBD that α-syn forms neuronal inclusions called Lewy bodies, in MSA, α-syn forms oligodendroglia GCI and suggest much higher levels than PD and DLBD(Tong et al., 2010). Most importantly, MSA suggest much higher level of soluble α-syn(Tong et al., 2010), conversely, PD and DLBD have higher levels of insoluble α-syn(Klucken et al., 2006). However, the implications and reasons for the different expression pattern of α-syn still remains unclear(Ubhi et al., 2011), it may lead to the different pathological processes and propagation model of α-syn in MSA.

Since the origin of αSyn that composes GCIs in oligodendrocytes remains enigmatic, the presence of neuronal protein α-syn in oligodendrocyte of MSA has drawn a lot of attention, especially many existing studies have reported no alterations in α-syn mRNA levels between the brains of control and MSA patients(Miller et al., 2005; Ozawa et al., 2001). One possible hypothesis of the abnormal oligodendroglial expression of α-syn is that α-syn may propagate from one cell to another(Kordower et al., 2008; Lee et al., 2010b). At the same time, glial cells are reported to endocytose α-syn from the media and transmit it to neighboring cells and the glial pathology is produced by direct transmission of neuronal α-syn aggregates(Lee et al., 2010a). Moreover, in AAV-hua-syn-injected rats, GCIs in oligodendrocytes were causing by the transmitting of α-syn form neurons(Reyes et al., 2014). Thus, neuronal αSyn transfer to oligodendrocytes helps our understanding of how MSA begins and progresses.

Recent years, fatty acid proteins (FABPs), a family of transporter proteins for lipid trafficking remain to be important factors associate with motor and cognitive functions(Cheng et al., 2021; Jia et al., 2021; Shioda et al., 2014). In dopamine neurons, the FABP3 regulates dopamine D2L receptor functions(Shioda et al., 2010) but accelerated α-syn oligomerization in 1-methyl-1,2,3,6-tetrahydropiridine (MPTP) treated mice which involved in dopamine neuron loss(Shioda et al., 2014). Consistently, in our previous work, we also found that FABP7 which only express in glia cells forms hetero-oligomers and aggregates with α-syn in oligodendrocytes(Cheng et al., 2022). At the same time, previous studies also suggested that FABP7 controlled lipid raft function by regulating caveolin-1 expression which may involve in endocytosis functions(Kagawa et al., 2015). Therefore, it is possible that FABP7 may involve in the pathological process of MSA and related to the expression pattern and propagation of α-syn in oligodendrocytes.

In this work, we focus on the potential role of FABP7 in α-syn accumulation and aggregation in oligodendrocyte and we also try to clarify the mechanism or propagation pattern of α-syn aggregates which closely related to demyelination, cell loss and MSA pathological process.

RESULT

FABP7 is involved in MSA pathology and α-syn aggregation

In our previous work, we reported that FABP7 formed high molecular weight oligomers and aggregates with α-syn in primary oligodendrocytes and glia cells(Cheng et al., 2022) and the aggregation and accumulation of α-syn in oligodendrocytes were considered as the most important cause of cell death in MSA. Here, to evaluate the role of FABP7 in MSA, we adopted one in vivo genetic model: PLP-hαSyn transgenic mice (PLP-hαSyn mice). The PLP--hαSyn mice bred on a C57/BL6 background exhibited phosphorylation of α-synuclein at Ser129 and aggregation of α-synuclein along with GCI-like inclusions (Figure 1A), which were widely used for study the pathological process of MSA(Kahle et al., 2002; Lee et al., 2019). To elucidate the molecular mechanisms underlying CNS dysfunction in MSA, the selected genes (P value ≤0.05) from the RNA sequencing analysis of the PLP-hαSyn mice brain (GSE129531) and whole blood of MSA patient (GSE34287)(Potashkin et al., 2012) were measured by GO_KEGG analysis. Consistent with previous work that the cerebellum ataxia is the second consensus statement on the diagnosis of multiple system atrophy(Gilman et al., 2008) (Figure S1A), in our result, the relationship between MSA and the olfactory transduction pathway as well as spinocerebellar ataxia pathway is very striking (Figure 1B). Then, focus on the cerebellum, we found obvious aggregation of hα-syn associated with FABP7 (Figure 1C) in PLP-hαSyn mice. Meanwhile, FABP7 also significantly decreased in the whole blood of MSA patient (Figure S1B). This result represents vital role of FABP7 in αSyn-dependent MSA pathology.

In order to a better understanding for the α-syn-related pathology in MSA, we stained whole brain of PLP-hαSyn mice with hαSyn antibody. Very interestingly, we found four regions including olfactory bulb, cortex, basial ganglia and cerebellum that the hαSyn are more prone to propagate (Figure 1D). In these regions, we also found the co-localization of hαSyn and FABP7 in oligodendrocytes (Figure 1E). However, it is unexpected that in cerebellum of PLP-hαSyn mice the purkinje neurons which express endogenous FABP7 also exhibited accumulation of hαSyn (Figure 1F). This accumulation may relate to the moto dysfunction and purkinje cell loss (Figure S2) in PLP-hαSyn mice.

In vitro, when we incubate the recombinant protein hαSyn and His-hfabp7 in Tris-HCl buffer at 37℃, with the extension of incubation time we found a rise in hαSyn levels at high molecular weights. Importantly, at the presence of His-hfabp7 the hαSyn bond to His-hfabp7 and forms much larger aggregates especially after 2 days incubation (Figure 1G). Since the presence of FABP7 altered the express pattern and molecular weight of αSyn aggregates, it is quite necessary to determine the differences of the two aggregates, in other word, to determine which pattern is more toxic. Thus, in this work, we also isolated the high molecular weight fractions (molecular weight > 100 kDa) by Ultracel-100 regenerated cellulose membrane (Figure 1H), and the aggregates were divided into two part (molecular weight > 100 kDa or < 100 kDa) (Figure 1I). Then, to understand the differences of toxicity, we treated the isolated proteins respectively into KG-1C human oligodendroglial cell line and measured the cell viability. As result, the cells treated with hαSyn in low molecular weight (molecular weight < 100 kDa) suggested no significant change in cell viability, however, the cells treated with hαSyn/His-hFABP7 in low molecular weight (molecular weight < 100 kDa) suggested decreased cell viability (Control vs

hαSyn/His-hFABP7 aggregates; MW<100kDa, n=6, $p < 0.05$, F (2, 15)=8.055). Importantly, both the cells treated with hαSyn (Control vs hαSyn aggregates; MW > 100kDa, n=6, $p < 0.05$, F (2, 15)=18.31) and hαSyn/His-hFABP7 (Control vs hαSyn/His-hFABP7 aggregates; MW > 100kDa, n=6, $p < 0.01$) in high molecular wight (molecular weight > 100 kDa) suggested decreased cell viability, but the cells treated with hαSyn/His-hFABP7 in high molecular wight (molecular weight > 100 kDa) suggested much lower cell viability than the hαSyn treated cells (hαSyn aggregates; MW > 100kDa vs hαSyn/His-hFABP7 aggregates; MW > 100kDa, n=6, $p < 0.05$) (Figure 1J). Therefore, these results indicate that FABP7 not only forms aggregates together with αSyn but also regulates the toxicity of αSyn aggregates.

FABP7/α-syn hetero-aggregates are selectively taken-up by oligodendrocytes and purkinje neuron

Our results above already suggested that FABP7 forms higher molecular weight aggregates with α-syn than itself and the hetero-aggreates are more toxic. But it still unclear that how it works *in vivo*. Therefore, we further purified the hαSyn/His-hFABP7 aggregates and injected them into lateral ventricles (LV) of mouse (3 μg per mouse) (Figure 2A) to evaluate the toxicity and propagation of aggregates *in vivo*. After two months of aggregates injection, we firstly confirmed the stability of injected aggregates. The lysates from mouse brain were immunoprecipitated and immunoblotted with anti-6X-His and anti-α-syn antibodies, and we found a tight binding of the two proteins which mean that the FABP7/α-syn connection and aggregates are still stable enough after two months of injection (Figure 2B). Next, in whole brain staining with 6X-His antibody, we measured the distribution of aggregates after injection. Surprisingly, it is consistent with our results in PLP-hαSyn mice, the injected aggregates also tend to propagate to olfactory bulb, cortex, basial ganglia and cerebellum (Figure 2C). Since these regions play important role in cognition and motor functions, we furthermore performed behavioral tests. As result, in rotarod tasks at 4 and 8 weeks, we observed significant differences in hαSyn/His-hFABP7 aggregates injected mice (4 weeks: n=7, $p < 0.05$; 8 weeks: n=7, $p < 0.05$) and hαSyn aggregates injected mice at 8 weeks (8 weeks: n=7, $p < 0.05$) compared with control mice (Figure 2D). In beam walking tasks, we observed significant differences at 4 and 8 weeks in hαSyn/His-hFABP7 aggregates injected mice (4 weeks: n=7, $p < 0.05$; 8 weeks: n=7, $p < 0.01$) and hαSyn aggregates injected mice at 8 weeks (8 weeks: n=7, $p < 0.05$) when compared to control mice. However, we also observed significant differences in beam walking tasks at 8 weeks between hαSyn/His-hFABP7 aggregates injected mice and hαSyn aggregates injected mice (8 weeks: n=7, $p < 0.05$) (Figure 2E). However, in Y-maze task, we only observed significant difference in total arm entry (8 weeks: Control vs hαSyn/His-hFABP7 aggregates; MW > 100kDa, n=7, $p < 0.01$; hαSyn aggregates; MW > 100kDa vs hαSyn/His-hFABP7 aggregates; MW > 100kDa, n=7, $p < 0.05$) but observed no changes in alternation (Figure 2F, G). These results may indicate the hαSyn/His-hFABP7 aggregates produce more severe toxicity towards motor function than hαSyn aggregates, however, both the two patterns of aggregates suggested a lack of effects on cognitive function.

After hαSyn/His-hFABP7 aggregates injection for 2 months, the aggregates mainly propagate to 4 regions. In the four regions, we found that the aggregates were selectively up-taken by oligodendrocytes (Figure 2H). We next calculated the percentage of oligodendrocytes in total 6x His positive cells and we found that 100% of aggregates in olfactory bulb, 60% of aggregates in cortex, 37% of aggregates in basal ganglia, 10% of aggregates in cerebellum were taken up by oligodencrotyes (Figure 2I). Even though the relatively low levels of aggregates were taken up by oligodencrotyes in cerebellum, the levels of MBP in white matter of cerebellum deceased significantly in hαSyn/His-hFABP7 aggregates injected mouse (Control mouse vs Injected mouse, n=6, $p < 0.01$) (Figure 2J, K, L). Thus, we furthermore focused on the purkinje neurons and amazingly, we found significant decreased of the numbers of purkinje neurons (Control mouse vs Injected mouse, n=6, $p < 0.01$) accompanied by accumulation of hαSyn/His-hFABP7 aggregates (Control mouse vs PLP mouse, n=6, $p < 0.01$) compared with control mouse (Figure 2M, N). Therefore, these results indicate that FABP7/α-syn hetero-aggregates are distinct pattern of αSyn aggregation which suggests higher toxicity towards oligodendrocytes and purkinje neuron due to the selectively uptake.

Scanning for potential receptors which regulating FABP7/α-syn hetero-aggregates propagation.

Till now, we already identified the role of FABP7 in α-syn aggregates formation and regulating higher toxicity towards oligodendrocytes and purkinje neurons due to the unknown mechanism, that these cells take up the FABP7/α-syn hetero-aggregates selectively. It is very reminiscent of a specific receptor that selectively modulates the FABP7/α-syn hetero-aggregates propagation and may closely connect with MSA pathological process. Interestingly, in previous work, FABP7 was also reported controls lipid raft function through the regulation of caveolin-1 expression in astrocyte(Kagawa et al., 2015). Thus, considering the important role of FABP7 in aggregation, we next performed a transcriptomic profile analysis of datasets to clarify candidate genes. Our research identified 20 genes significantly changed in all datasets (Figure 3A). However, the single-cell sequencing data from Sequence Read Archive (SRA) (GSM3449587)(Tepe et al., 2018; Ung et al., 2021) suggested only 6 genes (ENP2, FOXO3, KRT4, SLC27A3, SLC1A2 and RAB27B) express in both oligodendrocytes and purkinje neurons (Figure 3B,C; Figure S5). Next, in the result of protein-protein correlation analysis, we found the gene FABP7 and EPN2, which relate to cell endocytosis(Langridge and Struhl, 2017) are strongly correlated (Figure 3D). Interestingly, the mRNA expression of ENP2 was consistently downregulated in the whole blood of MSA patient with FABP7 form RNA-seq analyses data (GSE34287)(Potashkin et al., 2012) (Figure 3E).

For further identify whether the gene ENP2 really involved in FABP7/α-syn hetero-aggregates propagation, we firstly immunoprecipitated the protein epsin-2, which encoded by ENP2 gene and FABP7. As result, epsin-2 binds with both FABP7 and α-syn in both control mice and PLP-hαSyn mouse (Figure 3F). This result corroborated our hypothesis that epsin-2 involved in regulating FABP7/α-syn hetero-aggregates propagation. Then, we verified the cellular distribution of epsin-2 in brain using immunostaining. As result, the protein epsin-2 only express in oligodendrocyte (Figure 3G) and purkinje neurons (Figure S4B). On the other hand, despite the high basic level of epsin-2 in cerebellum and olfactory bulb of control mouse, we found an increased levels of MBP and epsin-2 merged areas in basal ganglia (Control mouse vs PLP mouse,

n=6, $p < 0.01$) and cortex (Control mouse vs PLP mouse, n=6, $p < 0.01$) of PLP-hαSyn mouse (Figure 3H). Very interestingly, the epsin-2 levels are very consistent with the levels of FABP7/α-syn hetero-aggregates in our injection mice. Therefore, these results indicate the close links between epsin-2 and FABP7 as well as aggregates, the epsin-2 may play underlying role in FABP7/α-syn hetero-aggregates propagation.

Knock down of epsin-2 decreased FABP7/α-syn hetero-aggregates uptake.

When we injected FABP7/α-syn hetero-aggregates into lateral ventricles, the injected mice exhibited moto dysfunction after four weeks and the demyelination or loss of purkinje neurons mainly occurred in cerebellum. Thus, here, we chose cerebellum injection with FABP7/α-syn hetero-aggregates (2 μg per mouse). Otherwise, to identify the role of epsin-2 in FABP7/α-syn hetero-aggregates propagation, we also injected mouse with virus (pAAV- mEPN2 shRNA-EGFP-U6) to knock down epsin-2 levels. In virus injection mice, virus was injected 2 weeks before aggregates injection and the motor functions were measured by beam-walking task and rotarod task once a week (Figure 4A, B). As result, In beam walking tasks, we observed significant differences at 1, 2 and 3 weeks in hαSyn/His-hFABP7 aggregates injected mice (1 week: Control vs aggregates injection, n=5, $p < 0.01$; 2 week: Control vs aggregates injection, n=5, $p < 0.01$; 3 week: Control vs aggregates injection, n=5, $p < 0.01$) compared to control mice. Meanwhile, in rotarod tasks, we also observed significant differences at 1, 2 and 3 weeks in hαSyn/His-hFABP7 aggregates injected mice (1 week: Control vs aggregates injection, n=5, $p < 0.05$; 2 week: Control vs aggregates injection, n=5, $p < 0.01$; 3 week: Control vs aggregates injection, n=5, $p < 0.01$) compared to control mice (Figure 4C). However, unfortunately, we did not observe significant changes that virus injection improves the motor functions in both beam-walking task and rotarod task within 3 weeks (Figure 4C).

On the other hand, even though the virus injection did not suggest significant effect on behaviors which may because of the very limited area of virus infection, in the infected area we found decreased levels of hαSyn/His-hFABP7 aggregates in oligodendrocytes (Aggregates Injection mouse vs Aggregates + AAV Injection mouse, n=5, $p < 0.01$) and purkinje neurons (Aggregates Injection mouse vs Aggregates + AAV Injection mouse, n=5, $p < 0.01$) followed decreased levels of episn-2 (Figure 4D, E). Furthermore, in the oligodendrocyte precursor cells (OPCs) primary culture, the virus infected cells also suggested significant decreased levels of hαSyn/His-hFABP7 aggregates uptake (Figure S6). Thus, even though the mechanism remains unclear, these results proved that epsin-2 regulated hαSyn/His-hFABP7 aggregates uptake in oligodendrocytes and purkinje neurons, it is a novel and potential therapeutic target for inhibiting αSyn accumulation and propagation in MSA.

DISCUSSION

On the basis of clinical features, MSA is divided into two main types: the parkinsonian type (MSA-P) with poor levodopa responsive parkinsonian syndrome and cerebellar type (MSA-C) with cerebellar ataxia syndrome (Ortiz et al., 2020). In MSA-C, the degree of morphological changes in cerebellum is more pronounced than MSA-P(Rusholt et al., 2020) as well as the

purkinje neuron dysfunctions include the increase of torpedoes in purkinje axonal morphology and reduction in dendritic spines of purkinje dendritic arbor have implicated cerebellar dysfunction(Kuo et al., 2017). Moreover, the loss of purkinje neurons and increased levels of GCIs in cerebellum of MSA patients may collected with demyelination and disease progression(Brettschneider et al., 2017). Consistently, in our work, we also observed obvious accumulations of αSyn in purkinje neurons and oligodendrocytes in the white matter of cerebellum in both PLP-hαSyn mice and hαSyn/His-hFABP7 aggregates injected mice. Considering the hαSyn, which only primarily expresses in oligodendrocytes in PLP-hαSyn mice also expresses in purkinje neurons, there must be some unknown mechanisms, which regulate αSyn propagation. In MSA patient, there is strong evidence that αSyn accumulation in oligodendrocytes result in the loss of myelin and oligodendroglial dysfunction(Wenning et al., 2008) within the pons and cerebellum relate to GCI pathology and disease duration(Ishizawa et al., 2008). Meanwhile, associated with GCI burden and demyelination, the purkinje neurons loss is another important cerebellar feature of MSA-C(Louis et al., 2014; Rusholt et al., 2020). Thus, the purkinje neuron loss seems to be a secondary consequence of αSyn accumulation and demyelination. We hypothesis that expect for the neuroinflammation in MSA-C (Hoffmann et al., 2019)induced by demyelination, the direct propagation of αSyn from oligodendrocytes to purkinje neurons is also an important incentive for purkinje neuron degeneration.

Since the origins of distinct αSyn-related diseases such as PD and MSA remains unclear, it is possible that distinct conformations of αSyn aggregates result in different disorders(Peelaerts et al., 2015; Prusiner et al., 2015; Tanudjojo et al., 2021). Different of PD brain, the MSA brain contains soluble activity and the αSyn form MSA brain induces distinct inclusion morphologies (Yamasaki et al., 2019). Consistently, different from the insoluble αSyn amyloid fibrils in PD brain, in our work the FABP7/α-syn hetero aggregates constructed by 2-days-incubation of recombinant protein are soluble. Due to the limitations of our experimental conditions, we cannot conclude that the pattern of αSyn aggregation in MSA brain is the same with the FABP7/α-syn hetero-aggregates in cerebellum of PLP-hαSyn mice, however, the way of FABP7/α-syn hetero-aggregates propagation is completely different from αSyn amyloid fibrils. In previous studies, the α-syn preformed fibrils (PFFs) treatment led to accumulations of α-syn in dopamine neurons and selective decreases in synaptic protein(Volpicelli-Daley et al., 2011) as well as motor deficits(Luk et al., 2012). In contrast, in the present study, the FABP7/α-syn hetero-aggregates only propagate to oligodendrocytes and purkinje neurons in both PLP-hαSyn mice and FABP7/α-syn hetero-aggregates injected mice. Obviously, the specific receptor for the propagation of distinct αSyn stains into different regions in CNS is necessary.

αSyn is an intracellular, cytosolic protein, for the propagation of αSyn to additional brain regions, the aggregates must bind to the cell surface and gain entry to the cytoplasm. The previous study has indicated dopamine D2 long receptors are critical for αSyn uptake(Kawahata et al., 2021) towards dopamine neurons. In the present study, we found the protein epsin-2 as one potential receptor which regulating the propagation of aggregates in MSA. Epsin-2 is one of endocytic adapter proteins, which contain an N-terminal ENTH domain and predicted unfolded central and C-terminal regions containing binding sites for clathrin(Chen et al., 2009). Otherwise, clathrin does not bind to plasma membrane directly, epsin-2 is ubiquitous components of endocytic clathrin-coated pits that interact with lipids on the plasma membrane(Garcia-Alai et al., 2018).

Here, in RNA sequencing analysis, we found the EPN2 gene strongly correlated with FABP7 and significantly changed in the whole blood of MSA patient. By immunostaining and immunoprecipitation analysis, we also demonstrated that epsin-2 regulated FABP7/α-syn hetero-aggregates propagation towards oligodendrocytes and purkinje neurons. However, in our epsin-2 knock-down mice which infected with virus did not exhibit the improvement of motor functions may because of the limited area of virus infection. Therefore, it is necessary for us to validate our experimental results with inhibitors of epsin-2 in our future work.

Overall, in this work we verified the vital role of FABP7 in α-syn aggregation in MSA by PLP-hαSyn mice, and we found out the special propagation pattern of FABP7/α-syn hetero-aggregates that selectively propagate to oligodendrocytes and purkinje neurons. Importantly, the protein epsin-2 is a novel receptor which is proved regulating FABP7/α-syn hetero-aggregates propagating. Therefore, epsin-2 is a potential MSA therapeutic target, and the development of inhibitors is necessary and meaningful.

LIMITATIONS OF THE STUDY

In this work, we only demonstrate our hypothesis in preclinical studies using MSA model mice, we lack clinical evidence to support our hypothesis that FABP7 is involved in α-syn aggregation of GCI formation directly in MSA brain. On the other hand, epsin-2 knock-down mice which infected with virus did not exhibit the improvement of motor functions may because of the limited area of virus infection. It is a pity that, so far, none of the specific episn-2 inhibitors can be obtained from the market. Thus, we are planning to clarify the mechanism and binding site for epsin-2 to regulate α-syn propagation and furthermore develop specific ligands for epsin-2 inhibitrion in our future work.

ACKNOWLEDGMENTS

We thank the Uehara Memorial Foundation and the Japan Agency for Medical Research and Development (AMED) (grant numbers JP17dm0107071, JP18dm0107071, JP19dm0107071, and JP20dm0107071) for the financial support provided.

AUTHOR CONTRIBUTIONS

An Cheng, data acquisition and original draft writing; Yifei Wang, recombinant protein purification; Tomoki Sekimori, methodology; Wenbin Jia, methodology; Yi Chen, methodology; David I Finkelstein, animals; Ichiro Kawahata, methodology; Takuya Sasaki and Kohji Fukunaga, supervision, project administration, funding, and reviewing and editing the manuscript. All authors critically reviewed the manuscript and approved the final version of the manuscript. A. Cheng and K. Fukunaga verified the data and had final responsibility for the decision to submit for publication.

DECLARATION OF INTERESTS

The authors have declared that no conflict of interest exists.

REFERENCE:

Brettschneider, J., Irwin, D.J., Boluda, S., Byrne, M.D., Fang, L., Lee, E.B., Robinson, J.L., Suh, E., Van Deerlin, V.M., Toledo, J.B., *et al.* (2017). Progression of alpha-synuclein pathology in multiple system atrophy of the cerebellar type. Neuropathol Appl Neurobiol *43*, 315-329.

Chen, H., Ko, G., Zatti, A., Di Giacomo, G., Liu, L., Raiteri, E., Perucco, E., Collesi, C., Min, W., Zeiss, C., *et al.* (2009). Embryonic arrest at midgestation and disruption of Notch signaling produced by the absence of both epsin 1 and epsin 2 in mice. Proc Natl Acad Sci U S A *106*, 13838-13843.

Chen, Y., Balasubramaniyan, V., Peng, J., Hurlock, E.C., Tallquist, M., Li, J., and Lu, Q.R. (2007). Isolation and culture of rat and mouse oligodendrocyte precursor cells. Nature Protocols *2*, 1044-1051.

Cheng, A., Jia, W., Kawahata, I., and Fukunaga, K. (2021). A novel fatty acid-binding protein 5 and 7 inhibitor ameliorates oligodendrocyte injury in multiple sclerosis mouse models. EBioMedicine *72*, 103582.

Cheng, A., Wang, Y.-f., Shinoda, Y., Kawahata, I., Yamamoto, T., Jia, W.-b., Yamamoto, H., Mizobata, T., Kawata, Y., and Fukunaga, K. (2022). Fatty acid-binding protein 7 triggers α-synuclein oligomerization in glial cells and oligodendrocytes associated with oxidative stress. Acta Pharmacologica Sinica *43*, 552-562.

Fanciulli, A., and Wenning, G.K. (2015). Multiple-System Atrophy. New England Journal of Medicine *372*, 249-263.

Franzén, O., Gan, L.M., and Björkegren, J.L.M. (2019). PanglaoDB: a web server for exploration of mouse and human single-cell RNA sequencing data. Database (Oxford) *2019*.

Garcia-Alai, M.M., Heidemann, J., Skruzny, M., Gieras, A., Mertens, H.D.T., Svergun, D.I., Kaksonen, M., Uetrecht, C., and Meijers, R. (2018). Epsin and Sla2 form assemblies through phospholipid interfaces. Nature Communications *9*, 328.

Gilman, S., Wenning, G.K., Low, P.A., Brooks, D.J., Mathias, C.J., Trojanowski, J.Q., Wood, N.W., Colosimo, C., Dürr, A., Fowler, C.J., *et al.* (2008). Second consensus statement on the diagnosis of multiple system atrophy. Neurology *71*, 670-676.

Hoffmann, A., Ettle, B., Battis, K., Reiprich, S., Schlachetzki, J.C.M., Masliah, E., Wegner, M., Kuhlmann, T., Riemenschneider, M.J., and Winkler, J. (2019). Oligodendroglial α-synucleinopathy-driven neuroinflammation in multiple system atrophy. Brain Pathol *29*, 380-396.

Ishizawa, K., Komori, T., Arai, N., Mizutani, T., and Hirose, T. (2008). Glial cytoplasmic inclusions and tissue injury in multiple system atrophy: A quantitative study in white matter (olivopontocerebellar system) and gray matter (nigrostriatal system). Neuropathology *28*, 249-257.

Jia, W., Wilar, G., Kawahata, I., Cheng, A., and Fukunaga, K. (2021). Impaired Acquisition of Nicotine-Induced Conditioned Place Preference in Fatty Acid-Binding Protein 3 Null Mice. Molecular Neurobiology *58*, 2030-2045.

Kagawa, Y., Yasumoto, Y., Sharifi, K., Ebrahimi, M., Islam, A., Miyazaki, H., Yamamoto, Y., Sawada, T., Kishi, H., Kobayashi, S., *et al.* (2015). Fatty acid-binding protein 7

regulates function of caveolae in astrocytes through expression of caveolin-1. Glia *63*, 780-794.
Kahle, P.J., Neumann, M., Ozmen, L., Muller, V., Jacobsen, H., Spooren, W., Fuss, B., Mallon, B., Macklin, W.B., Fujiwara, H., *et al.* (2002). Hyperphosphorylation and insolubility of alpha-synuclein in transgenic mouse oligodendrocytes. EMBO Rep *3*, 583-588.
Kawahata, I., Sekimori, T., Wang, H., Wang, Y., Sasaoka, T., Bousset, L., Melki, R., Mizobata, T., Kawata, Y., and Fukunaga, K. (2021). Dopamine D2 Long Receptors Are Critical for Caveolae-Mediated α-Synuclein Uptake in Cultured Dopaminergic Neurons. Biomedicines *9*, 49.
Klucken, J., Ingelsson, M., Shin, Y., Irizarry, M.C., Hedley-Whyte, E.T., Frosch, M., Growdon, J., McLean, P., and Hyman, B.T. (2006). Clinical and biochemical correlates of insoluble alpha-synuclein in dementia with Lewy bodies. Acta Neuropathol *111*, 101-108.
Kordower, J.H., Chu, Y., Hauser, R.A., Freeman, T.B., and Olanow, C.W. (2008). Lewy body-like pathology in long-term embryonic nigral transplants in Parkinson's disease. Nat Med *14*, 504-506.
Kuo, S.H., Lin, C.Y., Wang, J., Sims, P.A., Pan, M.K., Liou, J.Y., Lee, D., Tate, W.J., Kelly, G.C., Louis, E.D., *et al.* (2017). Climbing fiber-Purkinje cell synaptic pathology in tremor and cerebellar degenerative diseases. Acta Neuropathol *133*, 121-138.
Langridge, P.D., and Struhl, G. (2017). Epsin-Dependent Ligand Endocytosis Activates Notch by Force. Cell *171*, 1383-1396.e1312.
Lee, H.-J., Ricarte, D., Ortiz, D., and Lee, S.-J. (2019). Models of multiple system atrophy. Experimental & Molecular Medicine *51*, 1-10.
Lee, H.J., Suk, J.E., Patrick, C., Bae, E.J., Cho, J.H., Rho, S., Hwang, D., Masliah, E., and Lee, S.J. (2010a). Direct transfer of alpha-synuclein from neuron to astroglia causes inflammatory responses in synucleinopathies. J Biol Chem *285*, 9262-9272.
Lee, S.J., Desplats, P., Sigurdson, C., Tsigelny, I., and Masliah, E. (2010b). Cell-to-cell transmission of non-prion protein aggregates. Nat Rev Neurol *6*, 702-706.
Louis, E.D., Kuo, S.H., Vonsattel, J.P., and Faust, P.L. (2014). Torpedo formation and Purkinje cell loss: modeling their relationship in cerebellar disease. Cerebellum *13*, 433-439.
Luk, K.C., Kehm, V., Carroll, J., Zhang, B., O'Brien, P., Trojanowski, J.Q., and Lee, V.M. (2012). Pathological α-synuclein transmission initiates Parkinson-like neurodegeneration in nontransgenic mice. Science *338*, 949-953.
Miller, D.W., Johnson, J.M., Solano, S.M., Hollingsworth, Z.R., Standaert, D.G., and Young, A.B. (2005). Absence of alpha-synuclein mRNA expression in normal and multiple system atrophy oligodendroglia. J Neural Transm (Vienna) *112*, 1613-1624.
Ortiz, J.F., Betté, S., Tambo, W., Tao, F., Cozar, J.C., and Isaacson, S. (2020). Multiple System Atrophy - Cerebellar Type: Clinical Picture and Treatment of an Often-Overlooked Disorder. Cureus *12*, e10741.
Ozawa, T., Okuizumi, K., Ikeuchi, T., Wakabayashi, K., Takahashi, H., and Tsuji, S. (2001). Analysis of the expression level of alpha-synuclein mRNA using postmortem

brain samples from pathologically confirmed cases of multiple system atrophy. Acta Neuropathol *102*, 188-190.
Peelaerts, W., Bousset, L., Van der Perren, A., Moskalyuk, A., Pulizzi, R., Giugliano, M., Van den Haute, C., Melki, R., and Baekelandt, V. (2015). α-Synuclein strains cause distinct synucleinopathies after local and systemic administration. Nature *522*, 340-344.
Potashkin, J.A., Santiago, J.A., Ravina, B.M., Watts, A., and Leontovich, A.A. (2012). Biosignatures for Parkinson's disease and atypical parkinsonian disorders patients. PLoS One *7*, e43595.
Prusiner, S.B., Woerman, A.L., Mordes, D.A., Watts, J.C., Rampersaud, R., Berry, D.B., Patel, S., Oehler, A., Lowe, J.K., Kravitz, S.N., *et al.* (2015). Evidence for α-synuclein prions causing multiple system atrophy in humans with parkinsonism. Proc Natl Acad Sci U S A *112*, E5308-5317.
Reyes, J.F., Rey, N.L., Bousset, L., Melki, R., Brundin, P., and Angot, E. (2014). Alpha-synuclein transfers from neurons to oligodendrocytes. Glia *62*, 387-398.
Rusholt, E.H.L., Salvesen, L., Brudek, T., Tesfay, B., Pakkenberg, B., and Olesen, M.V. (2020). Pathological changes in the cerebellum of patients with multiple system atrophy and Parkinson's disease-a stereological study. Brain Pathol *30*, 576-588.
Schindelin, J., Arganda-Carreras, I., Frise, E., Kaynig, V., Longair, M., Pietzsch, T., Preibisch, S., Rueden, C., Saalfeld, S., Schmid, B., *et al.* (2012). Fiji: an open-source platform for biological-image analysis. Nature Methods *9*, 676-682.
Shioda, N., Yabuki, Y., Kobayashi, Y., Onozato, M., Owada, Y., and Fukunaga, K. (2014). FABP3 protein promotes α-synuclein oligomerization associated with 1-methyl-1,2,3,6-tetrahydropiridine-induced neurotoxicity. J Biol Chem *289*, 18957-18965.
Shioda, N., Yamamoto, Y., Watanabe, M., Binas, B., Owada, Y., and Fukunaga, K. (2010). Heart-type fatty acid binding protein regulates dopamine D2 receptor function in mouse brain. J Neurosci *30*, 3146-3155.
Spillantini, M.G., Crowther, R.A., Jakes, R., Cairns, N.J., Lantos, P.L., and Goedert, M. (1998). Filamentous alpha-synuclein inclusions link multiple system atrophy with Parkinson's disease and dementia with Lewy bodies. Neurosci Lett *251*, 205-208.
Spillantini, M.G., Schmidt, M.L., Lee, V.M.Y., Trojanowski, J.Q., Jakes, R., and Goedert, M. (1997). α-Synuclein in Lewy bodies. Nature *388*, 839-840.
Tanudjojo, B., Shaikh, S.S., Fenyi, A., Bousset, L., Agarwal, D., Marsh, J., Zois, C., Heman-Ackah, S., Fischer, R., Sims, D., *et al.* (2021). Phenotypic manifestation of α-synuclein strains derived from Parkinson's disease and multiple system atrophy in human dopaminergic neurons. Nat Commun *12*, 3817.
Tepe, B., Hill, M.C., Pekarek, B.T., Hunt, P.J., Martin, T.J., Martin, J.F., and Arenkiel, B.R. (2018). Single-Cell RNA-Seq of Mouse Olfactory Bulb Reveals Cellular Heterogeneity and Activity-Dependent Molecular Census of Adult-Born Neurons. Cell Rep *25*, 2689-2703.e2683.
Tong, J., Wong, H., Guttman, M., Ang, L.C., Forno, L.S., Shimadzu, M., Rajput, A.H., Muenter, M.D., Kish, S.J., Hornykiewicz, O., *et al.* (2010). Brain alpha-synuclein accumulation in multiple system atrophy, Parkinson's disease and progressive supranuclear palsy: a comparative investigation. Brain *133*, 172-188.

Ubhi, K., Low, P., and Masliah, E. (2011). Multiple system atrophy: a clinical and neuropathological perspective. Trends Neurosci *34*, 581-590.
Ung, K., Huang, T.W., Lozzi, B., Woo, J., Hanson, E., Pekarek, B., Tepe, B., Sardar, D., Cheng, Y.T., Liu, G., *et al.* (2021). Olfactory bulb astrocytes mediate sensory circuit processing through Sox9 in the mouse brain. Nat Commun *12*, 5230.
Volpicelli-Daley, L.A., Luk, K.C., Patel, T.P., Tanik, S.A., Riddle, D.M., Stieber, A., Meaney, D.F., Trojanowski, J.Q., and Lee, V.M. (2011). Exogenous α-synuclein fibrils induce Lewy body pathology leading to synaptic dysfunction and neuron death. Neuron *72*, 57-71.
Wenning, G.K., Stefanova, N., Jellinger, K.A., Poewe, W., and Schlossmacher, M.G. (2008). Multiple system atrophy: a primary oligodendrogliopathy. Ann Neurol *64*, 239-246.
Yamasaki, T.R., Holmes, B.B., Furman, J.L., Dhavale, D.D., Su, B.W., Song, E.S., Cairns, N.J., Kotzbauer, P.T., and Diamond, M.I. (2019). Parkinson's disease and multiple system atrophy have distinct α-synuclein seed characteristics. J Biol Chem *294*, 1045-1058.

METHODS

KEY RESOURCES TABLE

REAGENT or RESOURCE	Source	Identifiers
Antibodies		
Chicken Anti-MBP	EnCor Biotechnology	Cat#CPCA-MBP; RRID: AB_2572352
Goat Anti-FABP7	R&D Systems	Cat#AF3166; RRID: AB_2100475
Mouse Anti-β-tubulin	Sigma-Aldrich	Cat#T0198; RRID: AB_477556
Rabbit Anti-Olig2	Sigma-Aldrich	Cat#MABN50; RRID: AB_10807410
Mouse Anti-Human-αSyn	Gene Tex	Cat#GTX21904; RRID: AB_380341
Rabbit Anti-Calbindin	abcam	Cat#ab108404; RRID: AB_10861236
Mouse Anti-6X-His tag	abcam	Cat#ab18184; RRID: AB_444306
Rabbit Anti-NeuN	abcam	Cat#ab177487; RRID: AB_2532109
Rabbit Anti-GFAP	abcam	Cat#ab7260; RRID: AB_305808
Mouse Anti-Epsin-2	Santa Cruz Biotechnology	Cat#Cat#sc-376788; RRID: AB_2920722
Goat Anti-Mouse IgG(H+L), Human ads-HRP	SouthernBiotech	Cat#1031-05; RRID: AB 2794307
Goat Anti-Rabbit IgG (H&L) , Mouse/Human ads-HRP	SouthernBiotech	Cat#4050-05; RRID: AB 2795955

Goat anti-Mouse IgG (H+L) Cross-Adsorbed Secondary Antibody, Alexa Fluor™ 405	Thermo Fisher Scientific	Cat#A-31553; RRID: AB 221604
Donkey anti-Goat IgG (H+L) Cross-Adsorbed Secondary Antibody, Alexa Fluor™ 488	Thermo Fisher Scientific	Cat#A-11055; RRID: AB 2534102
Donkey anti-Mouse IgG (H+L) Highly Cross-Adsorbed Secondary Antibody, Alexa Fluor™ 594	Thermo Fisher Scientific	Cat#A-21203; RRID: AB 141633
Donkey anti-Rabbit IgG (H+L) Highly Cross-Adsorbed Secondary Antibody, Alexa Fluor™ 594	Thermo Fisher Scientific	Cat#A-21207; RRID: AB 141637
Chemicals, Cell line, virus, and Recombinant proteins		
KG-1-C human oligodendroglial cells	RIKEN BRC Cell Bank	RRID:CVCL_2971
D-MEM(High Glucose) with L-Glutamine, Phenol Red and Sodium Pyruvate	FUJIFILM	Cat#043-30085
pAAV[shRNA]-EGFP-U6>mEpn2	vectorbuilder	https://www.vectorbuilder.jp/
pAAV[shRNA]-EGFP-U6>Scramble	vectorbuilder	https://www.vectorbuilder.jp/
apo-Transferrin	Sigma-Aldrich	Cat#T2252
Insulin	Sigma-Aldrich	Cat#I6634
Sodium selenite	Sigma-Aldrich	Cat#s5261
D-Biotin	Sigma-Aldrich	Cat#aB4501
Penicillin/streptomycin	Invitrogen	Cat#15140
Poly-D-lysine	Sigma-Aldrich	Cat#P0899
DNase I	Sigma-Aldrich	Cat#D5025
bFGF	REPROCELL	Cat#RCHEOT002
L-Glutamine	Sigma-Aldrich	Cat#G8540
Fetal bovine serum	Hyclone	Cat# SH300700
Human PDGF-AA	Pepro tech	Cat#100-13A
Ethylenediaminetetraacetic acid	Sigma-Aldrich	Cat#E5134

disodium salt dihydrate		
Sodium dodecyl sulfate	Sigma-Aldrich	Cat#151-21-3
Triton™ X-100	Sigma-Aldrich	Cat#9036-19-5
Trypsin:L-1-tosylamido-2-phenylethylchloromethylketone(TPCK)-treated trypsin	Sigma-Aldrich	Cat#T1426
Sodium orthovanadate	Sigma-Aldrich	Cat#S6508
leupeptin	Sigma-Aldrich	Cat#L2884
Pepstatin A	Sigma-Aldrich	Cat#P5318
Sodium fluoride	Sigma-Aldrich	Cat#201154
Sodium pyrophosphate decahydrate	Sigma-Aldrich	Cat#221368
Sodium chloride	Sigma-Aldrich	Cat#S9888
E. coli DH5α Competent Cells & SOC medium	TaKaRa	Cat#9057
Isopropyl-β-D-thiogalactoside	Sigma-Aldrich	Cat#10724815001
Calyculin A	Sigma-Aldrich	Cat#C5552
Trypsin inhibitor	Sigma-Aldrich	Cat#T9003
DL-Dithiothreitol solution	Sigma-Aldrich	Cat#43816
Recombinant Human Alpha-synuclein protein	Abcam	Cat#ab51189
Critical Commercial Assays		
His-tagged recombinant protein purification—His60 Ni Gravity Columns	TaKaRa	Cat#635658
QIAGEN Plasmid Midi Kit	Qiagen	Cat#12143
In-Fusion® HD Cloning Kit	TaKaRa	Cat#Z9648N
TaKaRa PCR Amplification Kit	TaKaRa	Cat#R011
Software		
Fiji-ImageJ (version 2.1.0)	(Schindelin et al., 2012)	https://imagej.net/Fiji. RRID:SCR_003070
Prism(version8.4.0)	GraphPad	https://www.graphpad.com/scientificsoftware/prism/;RRID:SCR_002798

R (Versions 3.6.2–4.1.1)	The R Foundation	https://www.r-project.org/foundation/; RRID:SCR_001905

RESOURCE AVAILABILITY

Lead contact

Requests for further information should be directed to the lead contact, Kohji Fukunaga, Tohoku University, koji.fukunaga.c1@tohoku.ac.jp

Materials availability

The materials used in this study are available commercially.

Data and code availability

The data supporting the findings of this study are available in the article and/or supplementary materials. The data in figure 1B, figure S1 and figure 3A, D, E were based on publicly available data from the Gene Expression Omnibus (GEO; GSE129531, https://www.ncbi.nlm.nih.gov/geo/query/acc.cgi?acc=GSE129531; GSE34287(Potashkin et al., 2012), https://www.ncbi.nlm.nih.gov/geo/query/acc.cgi). The data in figure 3B, C and figure S6 were based on publicly available data from the Gene Expression Omnibus (GSM3449587(Tepe et al., 2018; Ung et al., 2021), https://www.ncbi.nlm.nih.gov/geo/query/acc.cgi?acc=GSE121891) and measured by PanglaoDB(Franzén et al., 2019) (https://panglaodb.se/#google_vignette). Readers are welcome to contact the corresponding author for the raw data used in this work.

EXPERIMENTAL MODEL AND SUBJECT DETAILS

Animals

Eight-week-old male C57BMF/6J mice (Clea Japan, Inc.; Tokyo, Japan) and PLP-hαSyn transgenic mice (The Jackson Laboratory) were maintained in polypropylene cages (temperature: 23±2°C; humidity: 55±5%; lights on between 9 a.m. and 9 p.m.). Animals had unlimited access to food and water. We used only male mice in this study, to minimize the effect of sex hormones such as estrogen. All animal experiments were reviewed and approved by the Institutional Animal Care and Use Committee of the Tohoku University Environmental and Safety Committee (2019PhLM0-021 and 2019PhA-024). All animal experiments were performed following the animal use guidelines and ethical approval. For each group, mice were treated and measured randomly, and there were no confounders. For anesthesia, isoflurane was used during experiment. For euthanasia, mice were injected with overdose of pentobarbital intraperitoneally.

Primary oligodendrocyte precursor cells (OPCs) culture

The method for primary OPCs culture had been described previously(Chen et al., 2007). Briefly, P1-2 mouse pups were decapitated, followed by isolation of the cortex from the brain and digestion in a digestion solution (13.6 mL PBS, 0·8 mL DNase I stock solution [0·2 mg/mL], and 0·6 mL of a trypsin stock solution [0·25%]). Then sliced the tissues into approximately 1 mm^3

chunks by sterilised razor blade, centrifuged at 100 × *g* for 5 min, and resuspended in DMEM20S medium (DMEM, 4 mM L-glutamine, 1 mM sodium pyruvate, 20% foetal bovine serum [FBS], 50 U/mL penicillin, and 50 μg/mL streptomycin). The tissue suspension was strained using a 70 μm nylon cell strainer, seeded in poly L-lysine-coated tissue culture flasks and cultured in DMEM20S medium for 2 weeks (mixed culture). After that the flasks were shaken for 1 h at 200 rpm at 37 °C to remove microglial cells, and for an additional 20 h to detach OPCs, and then seeded on poly-D-lysine-coated plates and cultured in OPC medium (DMEM, 4 mM L-glutamine, 1 mM sodium pyruvate, 0.1% BSA, 50 μg/mL Apo-transferrin, 5 μg/mL insulin, 30 nM sodium selenite, 10 nM D-biotin and 10 nM hydrocortisone 10 ng/mL PDGF-AA and 10 ng/mL bFGF).

Preparation of protein

FABP7 with N-terminal 6X His-tag (His-hFABP7) was expressed in E. coli DH5α Competent Cells by pET28a derived vector containing coding genes constructed by In-Fusion® HD Cloning Kit. is. The hFABP7 gene were inserted into pET28a using either the restriction sites NcoI and XhoI (hFABP7) or NdeI and XhoI (His-hFABP7). Expression vectors were confirmed by sequencing before use in expressing proteins. For protein purification, after transformed cells were grown to OD_{600}=0.6~0.8, cells were additionally incubated with 1 mM Isopropyl-β-D-thiogalactoside (IPTG, 1mM) for 15h at 37 ℃. Then, cells were centrifuged (5000 rpm, 10min, 4 ℃) and resuspended in Tris-HCl buffer (50mM Tris-HCl, pH=7.4 in a 10:- (w/v) ratio). Next, the resuspended cells were sonicated totally, after centrifugation (15000rpm, 10min, 4 ℃) the collected supernatant was brought to 80% saturation by solid ammonium sulfate. After that, the supernatant containing His-hFABP7 was resolubilized in Tris-HCl buffer (50mM Tris-HCl, pH=7.4). For His-hFABP7 extraction, we used His-tagged recombinant protein purification—His60 Ni Gravity Columns followed the manufacturer's instructions. After column development, we pooled the fractions containing His-hFABP7, and added 0.4-fold volume of solution, diisopropyl ether : n-butanol (3:2). The mixture was stand at 4 ℃ with gentle agitation (20 rpm) for three cycles of 30 min intervals. Moreover, the solution was desalted by sequential dialysis (5 mM, 3 mM, and 1 mM NH4HCO3) and finally lyophilized to obtain delipidized, lyophilized His-hFABP7 protein.

Aggregates construction

Purified His-hFABP7 (0.2 mg / ml), and hαSyn (0.2 mg / ml), obtained from abcam were incubated in Tris-HCl buffer (150 mM NaCl, 10 mM Tris, pH = 7.5) at 37 ° C for 2h, 24h, and 2 days. The binding of FABP7 and αSyn was confirmed by Western blotting. For separating aggregates fractions, the incubated protein mixture was collected and centrifuged using Centrifugal Filters Utracel-100K (Millipore) at 500 g for 10 minutes. Then the filter was washed with PBS and centrifuged again at 500 g for 10 minutes. Repeat it three times, the last residue on the filter is the aggregate with the molecular weight of over 100 kDa. Aggregates were desalted by sequential dialysis (5 mM, 3 mM, and 1 mM NH4HCO3) and finally lyophilized.

Cell culture

KG-1C human oligodendroglial cells (RRID: CVCL_2971) were obtained from the RIKEN BRC Cell Bank (Tsukuba, Japan). Short-tandem repeat (STR) profiling of cell lines was performed by

JCRB. Cells were cultured in Dulbecco's Modified Eagle Medium (DMEM) with 10% FBS and penicillin/streptomycin (100 U/100 μg/mL) at 37°C under 5% CO2.

Stereotactic injection

For intracerebroventricular injections, the same titer ($1.13x10^{13}$ GC/ml) and equal amounts (2 μL per side) of viral particles or constructed aggregates (3 μL per mouse) were injected into the lateral ventricle at the following coordinates (anterior—0.7 mm; lateral±1; depth—2.5 mm relative to the bregma) through a Hamilton syringe (Hamilton Company, Reno, NV, USA). For direct cerebellar injection, the same titer ($1.13x10^{13}$ GC/ml) and equal amounts (1 μL per mouse) of viral particles or constructed aggregates (1 μL per mouse) were injected into the cerebellum directly at the following coordinates (anterior—6 mm; lateral 0 mm; depth—2.8 mm relative to the bregma) through a Hamilton syringe (Hamilton Company, Reno, NV, USA).

Protein extraction from brain tissue

Frozen tissues were subjected to lysis buffer containing 0.5% Triton-X100, 4 mM ethylene glycol, 50 mM Tris-HCl (pH 7.4), 10 mM ethylenediaminetetraacetic acid, 1 mM sodium orthovanadate, 50 mM sodium fluoride, 40 mM sodium pyrophosphate decahydrate, 0.15 M sodium chloride, 50 μg / mL leupeptin, 25 μg / mL peptatin A, 50 μg / mL trypsin inhibitor, 100 nM cariculin A, 1 mM dithiothreitol. Then tissues were homogenized, and sonicated totally. After centrifugation (15000 rpm, 10min, 4 ℃), the supernatant protein was collected and the concentration was normalized using Bradford's assay. Then the samples were mixed with a 6 × Laemmli sample buffer containing no β-mercaptoethanol and treated at 100 ° C for about 3 minutes.

SDS-PAGE

Extracts (30 μg) were separated by SDS-polyacrylamide gel electrophoresis (SDS-PAGE) using a ready-made gel (Cosmo Bio Co., Ltd.) and transferred to a polyvinylidene fluoride membrane in a buffer containing 3.03 g/L Tris, 14.41 g/L glycine for 2 hours. The membrane was then blocked with 5% defatted milk powder in a TTBS solution containing 50 mM Tris–HCl (pH=7.5), 150 mM NaCl, and 0.1% Tween 20 for 1 hour. Membranes were incubated overnight with primary antibodies at 4 ° C. After washing 3 times with TTBS (10 minutes each time), the membrane was incubated with TTBS diluted secondary antibody for 2 hours at room temperature. The membrane was then incubated using an ECL detection system (Amersham Biosciences, NJ, USA) and then intensity quantification was performed using Image Gauge software version 3.41 (Fuji Film, Tokyo, Japan).

Slice and histochemistry

Mice were anesthetized with isoflurane and perfused with PBS followed by 4% PFA. The brain was fixed overnight with 4% PFA and sliced by cryostat (Leica) (Twenty-micron brain sections). Immunofluorescent staining was performed as previously described(Cheng et al., 2021). The slice was permeated for 5 minutes using 0.1% Triton X-100 in PBS and then washed 3 times (10 minutes each time) and blocked with PBS / 1% BSA for 1 hour respectively. The primary antibodies were incubated overnight in blocking solution at 4 ℃. After washing with PBS / 1% BSA three times, a fluorescent secondary antibody was attached. Finally, immunofluorescent

images were analyzed using a confocal laser scanning microscope (DMi8; Leica, Wetzlar, Germany).

Cell viability assay

Cell viability was measured using a cell counting kit (CCK) (Dojindo) according to the manufacturer's instructions. This assay is based on the clearance of the water-soluble tetrazolium salt WST-8. It is reduced by intracellular dehydrogenase activity to produce a yellow formazan pigment. This dye is soluble in tissue culture medium. Its absorbance by living cells is measured at 400 nm and 450 nm.

Y-maze task

Spatial memory was evaluated using a Y-maze task. A Y-shaped maze with three arms (50 cm long, 7.5 cm high, 10.5 cm wide) connected at an angle of 120 degrees was placed on the desk for use. The mouse was placed on the end of one arm, and allowed to explore the maze freely for 8 minutes, and the positions of the arms to which the mouse moved were recorded in the selected order. The number of times the mouse moved to each arm within the specified time was counted, and this was taken as the total number of arm selections. From this, we investigated the combination of three different arms selected in succession, and we were able to recognize this number as the number of alternating actions. In the quantitative calculation, the number of alternation actions is divided by the total number of arm selections minus 2, and the value obtained by multiplying the value by 100 is used to obtain the alternation action rate (Altenations (%)), which is used for voluntary alternation actions.

Rotarod task

A device consisting of iron rods (3 cm in diameter and 30 cm in length) machined to prevent slipping was used. In the test, the mouse was placed on a rotating rod at 30 rpm and the time to fall was recorded for up to 300 seconds.

Beam walking task

A (155 mm x 160 mm x 5 mm) "goal box" was placed at the top of a rectangular beam (length: 870 mm x width: 5 mm) and both ends of the beam were fixed at 500 and 315 mm from the floor. As a training action, the mice were placed 10, 30, 50, and 80 cm away from the goal and walked to the goal box. In the test, the mouse was placed 80 cm from the goal box and the number of miss steps to reach the goal box within 60 seconds was recorded.

Bioinformatics

The original RNA sequencing data of PLP-hαSyn mice and whole blood of MSA patient were obtained from Gene Expression Omnibus (GEO; GSE129531, https://www.ncbi.nlm.nih.gov/geo/query/acc.cgi?acc=GSE129531; GSE34287(Potashkin et al., 2012), https://www.ncbi.nlm.nih.gov/geo/query/acc.cgi) and (GSM3449587(Tepe et al., 2018; Ung et al., 2021), respectively. The data were processed through RStudio. The original data for single-cell sequencing were obtained from Sequence Read Archive (SRA) (GSM3449587)(Tepe et al., 2018; Ung et al., 2021) (https://www.ncbi.nlm.nih.gov/geo/query/acc.cgi?acc=GSE121891) and measured by PanglaoDB(Franzén et al., 2019) (https://panglaodb.se/#google_vignette).

Statistics

Data were analyzed using GraphPad Prism 8 (GraphPad Software, Inc., La Jolla, CA, USA) and are expressed as the mean ± standard error of the mean (SEM). The normality assumption was examined using the Shapiro-Wilk test, and the equal variance assumption was examined by the Brown-Forsythe test using GraphPad Prism 8. For the data that passed these assumptions, significant differences were determined using Student's t-test for two-group comparisons (Figure 2L; Figure 2N; Figure S2B ; Figure 3H; Figure 4E; Figure S4C; Figure S6C) and by one-way analysis of variance (ANOVA) or two-way analysis of variance (ANOVA) for other multigroup comparisons, followed by Tukey's multiple comparisons test. Statistical significance was set at $p < 0{\cdot}05$.

Figure legends

Figure 1: FABP7 related to MSA progression and participated in αSyn toxicity.

A, Scheme of PLP-hαSyn mice. B, KEGG analysis of pathways enriched for the genes that are more differentially expressed in the PLP-hαSyn mice brain. C, Western blot analysis of αSyn (left) and FABP7 (right) in cerebellum extracts of PLP-hαSyn mice. D, Confocal images show the distribution of αSyn (green) in whole brain of PLP-hαSyn mice. E, Confocal images show the colocalization of FABP7 (green), hαSyn (red), and Olig2 (blue) in the oligodendrocytes in olfactory bulb, cortex, basial ganglia and cerebellum of PLP-hαSyn mice. F, Confocal images show the colocalization of calbindin (green), hαSyn (red), and DAPI (blue) in cerebellum of PLP-hαSyn mice. (G) Western blot analysis of αSyn and FABP7, human-αSyn and human-FABP7 were incubated in Tris-HCl (10 mM, pH=7.5) for two days. (H) Scheme of the filter for separating recombinant proteins. (I) Western blot analysis of αSyn and FABP7, mixtures were separated two fractions, below 100 kDa or over 100 kDa. (J) Cell viability analysis of KG-1C cells, based on a CCK assay. Cells cultured treated with separated fractions at a final concentrations of 5 μg/ml, for 24 h. The data are presented as the mean ± the standard error of the mean, were obtained using and one-way analysis of variance. $^{\#}P < 0.05$, $^{*}P < 0.05$, and $^{**}P < 0.01$. αSyn, alpha-synuclein. FABP7, fatty acid binding protein 7; NS, nonesignificant.

Figure 2: FABP7/α-syn hetero-aggregates suggest motor nerve related toxicity *in vivo*.

A, Scheme of aggregates injection and experimental protocol, purified aggregates were injected into lateral ventricles for 3μg per mouse. B, Co-immunoprecipitation of 6X His-tag and αSyn in tissue lysates of olfactory bulb. Extracts were immunoprecipitated (IP) with anti-His or anti-αSyn antibody. The immunoprecipitates were then immunoblotted (IB) with anti-His antibody or with anti-αSyn antibody. As the control, His and αSyn immunoreactive bands, tissue extracts (Input) are shown on the left. C, Confocal images show the distribution of aggregates in whole brain (anti-6X His-tag) after injection for 8 weeks. D, E, F, G, Behavioral tasks were carried out at beginning and after aggregates injection for 2 weeks, 4 weeks and 8 weeks. H, Confocal images show the colocalization of Olig2 (green) and 6X His-tag (red) and FABP7 (blue) in

oligodendrocytes. (I) Quantification of the percentage of oligodendrocytes taken up aggregates. J, Confocal images show the decreased MBP levels in FABP7/α-syn hetero-aggregates injected cerebellum. K, Western blot analysis of MBP and β-tubulin. L, Quantification of K, suggested decreased MBP levels in FABP7/α-syn hetero-aggregates injected cerebellum. M, Confocal images show the accumulation of FABP7/α-syn hetero-aggregates (6X His-tag, red) in purkinje neurons (calbindin, green), DAPI (blue). N, Quantification of calbindin positive cells and calbindin/6X His-tag double positive cells, suggested decreased numbers of calbindin positive cells and increased numbers of calbindin/6X His-tag double positive cells. The data are presented as the mean ± the standard error of the mean, were obtained using student's t-test and two-way analysis of variance. *$P < 0.05$ and **$P < 0.01$. αSyn, alpha-synuclein; FABP7, fatty acid binding protein 7; MBP, myelin basic protein; NS, nonsignificant.

Figure 3: Scanning for potential receptors.

A, An overlapping Venn diagram of transcriptomic differential genes in two candidate gene databases. B, C, UMAP dimensional reduction visualizations of 5240 cells from olfactory bulb (mouse strain=C57BL/6NJ). Color represents normalized log expression of selected genes. Each point represents a cell. Original data were obtained from Gene Expression Omnibus (GEO; GSM3449587) and Sequencing data was handled using PanglaoDB (https://panglaodb.se/). Suggested that 6 genes (ENP2, FOXO3, KRT4, SLC27A3, SLC1A2 and RAB27B) express in both oligodendrocytes and purkinje neurons. D, protein-protein correlation analysis for selected six genes, revealing two specific interactions, marked with Star symbol. E, Volcano plot of the log2 fold change (n=3) on the X-axis and $\log^{10}$ of the p-value derived using two-way ANOVA. Each point represents an individual mRNA from PLP-hαSyn mice brain. Colored points represent significantly changed mRNA, and grey points represent non-significant mRNA ($p < 0.05$ and $|\log2\ FC| \geq 0.01$). F, Co-immunoprecipitation of Epsin-2 and FABP7 in tissue lysates of cerebellum. Extracts were immunoprecipitated (IP) with anti-Epsin-2 or anti-FABP7 antibody. The immunoprecipitates were then immunoblotted (IB) with anti-Epsin-2 antibody or with anti-FABP7 antibody. G, Confocal images show the distribution epsin-2 (red) in neuron (NeuN, green), astrocyte (GFAP, green), and oligodendrocyte (MBP, green), DAPI (blue). H, Quantification of G, suggested increased levels of MBP and epsin-2 merged areas in basal ganglia and cortex. The data are presented as the mean ± the standard error of the mean, were obtained using student's t-test. **$P < 0.01$. αSyn, alpha-synuclein; FABP7, fatty acid binding protein 7; MBP, myelin basic protein; NS, nonsignificant.

Figure 4: Knock down of epsin-2 decreased FABP7/α-syn hetero-aggregates uptake.

A, Scheme of aggregates, and AAV injection and experimental protocol. B, Confocal images show distribution of AAV (green), epsin-2 (red), and DAPI (blue) in cerebellum. C, Behavioral tasks were carried out at beginning and after aggregates or AAV injection for 1 week, 2 weeks and 3 weeks. D, Confocal images show the propagation of injected aggregates in cerebellum. E, Quantification of D, suggested decreased levels of hαSyn/His-hFABP7 aggregates uptake in purkinje neurons and oligodendrocytes in AAV injected mice. The data are presented as the mean ± the standard error of the mean, were obtained using student's t-test and two-way analysis

of variance *P < 0.05 and **P < 0.01. αSyn, alpha-synuclein; FABP7, fatty acid binding protein 7; MBP, myelin basic protein; NS, nonsignificant.

Epsin2, a novel target for multiple system atrophy therapy via regulating α-synuclein propagation associated with FABP7

An Cheng[1, 2, *], Yifei Wang[1], Tomoki Sekimori[2], Wenbin Jia[1, 2], Yi Chen[3], David I Finkelstein[4], Ichiro Kawahata[2], Takuya Sasaki[1, *], Kohji Fukunaga[2,5, *]

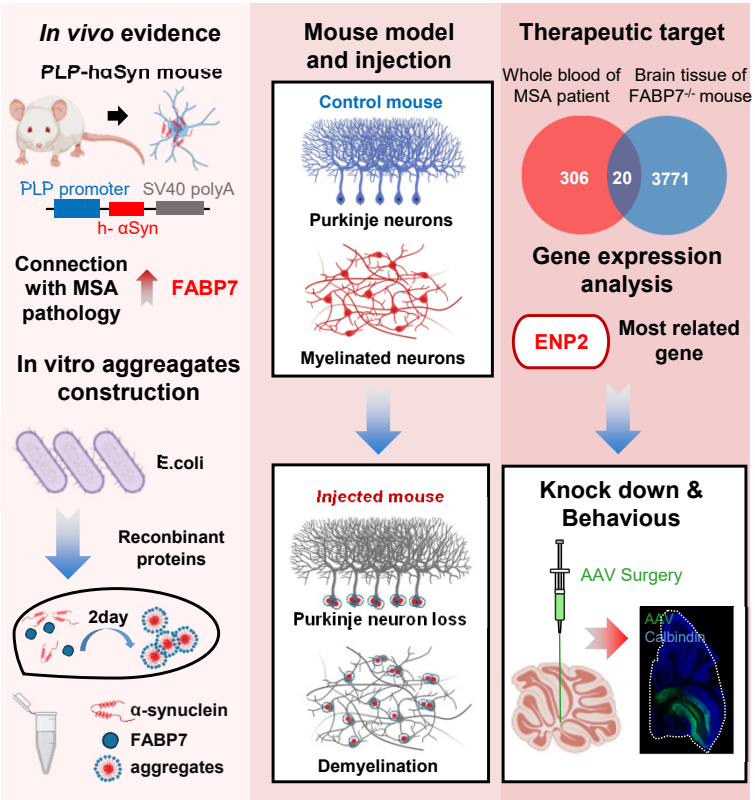

Graphical abstract

[1] Department of Pharmacology, Graduate School of Pharmaceutical Sciences, Tohoku University, Sendai, Japan

[2] Department of CNS Drug Innovation, Graduate School of Pharmaceutical Sciences, Tohoku University, Sendai, Japan

[3] Department of Industrial Engineering & Decision Analytics, Hong Kong University of Science and Technology, Hong Kong

[4] Mental Health Research Institute, The University of Melbourne, Victoria, Australia

[5] Lead contact

* Correspondence should be addressed to An Cheng (leon.an.cheng.1q84@gmail.com); Takuya Sasaki (t.sasaki.0224@gmail.com); Kohji Fukunaga (koji.fukunaga.c1@tohoku.ac.jp)

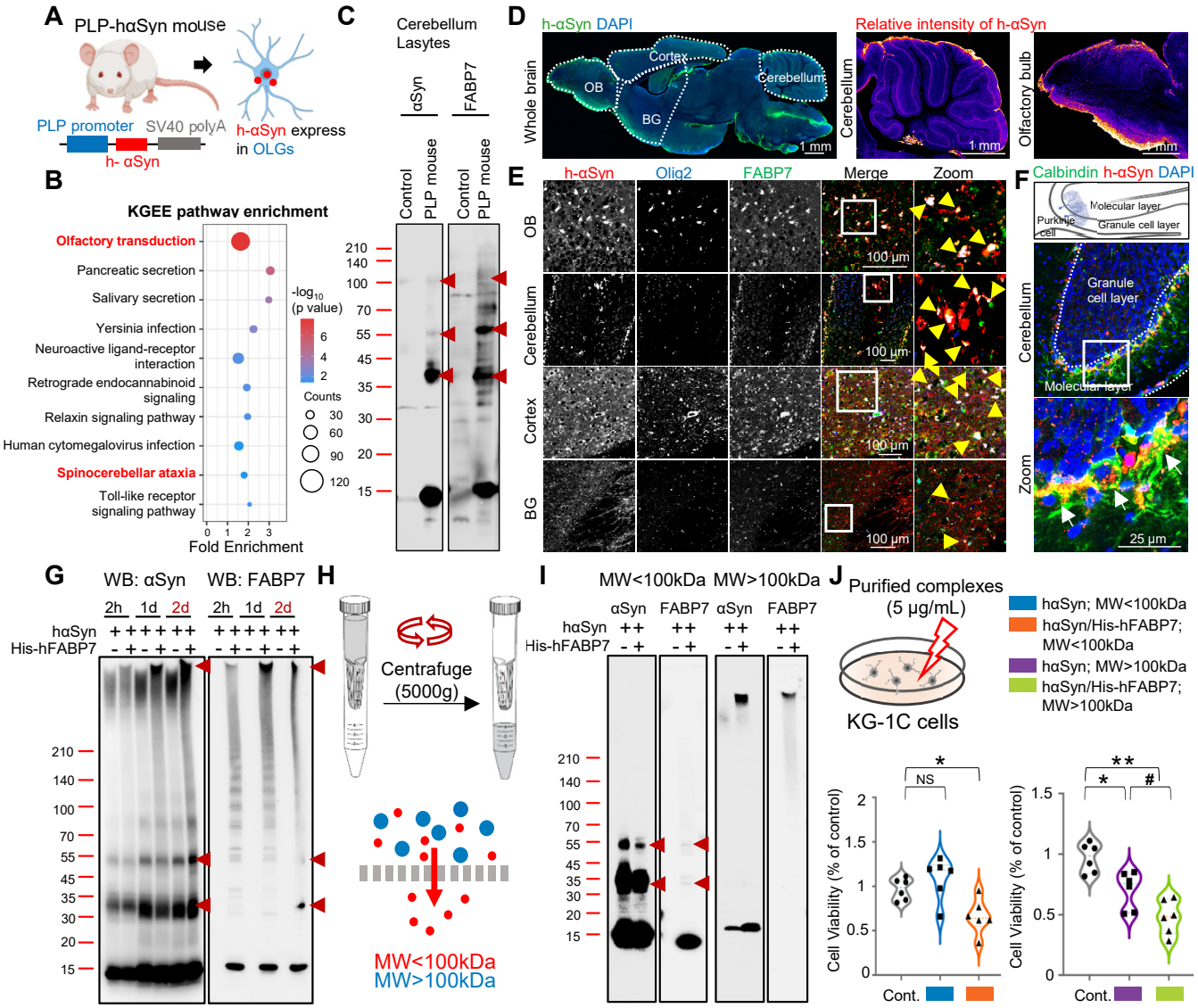
A
PLP-hαSyn mouse
PLP promoter
SV40 polyA
h- αSyn
h-αSyn express in OLGs
B
KGEE pathway enrichment
Olfactory transduction
Pancreatic secretion
Salivary secretion
Yersinia infection
Neuroactive ligand-receptor interaction
Retrograde endocannabinoid signaling
Relaxin signaling pathway
Human cytomegalovirus infection
Spinocerebellar ataxia
Toll-like receptor signaling pathway
-log10 (p value)
Counts
Fold Enrichment
C
Cerebellum Lasytes
αSyn
FABP7
Control
PLP mouse
D
h-αSyn DAPI
Relative intensity of h-αSyn
Whole brain
Cerebellum
Olfactory bulb
Cortex
OB
BG
1 mm
E
h-αSyn
Olig2
FABP7
Merge
Zoom
100 µm
F
Calbindin h-αSyn DAPI
Molecular layer
Purkinje cell
Granule cell layer
25 µm
G
WB: αSyn
WB: FABP7
2h
1d
2d
hαSyn
His-hFABP7
H
Centrafuge (5000g)
MW<100kDa
MW>100kDa
I
MW<100kDa MW>100kDa
J
Purified complexes (5 µg/mL)
KG-1C cells
hαSyn; MW<100kDa
hαSyn/His-hFABP7; MW<100kDa
hαSyn; MW>100kDa
hαSyn/His-hFABP7; MW>100kDa
Cell Viability (% of control)
NS
Cont.

Figure 1

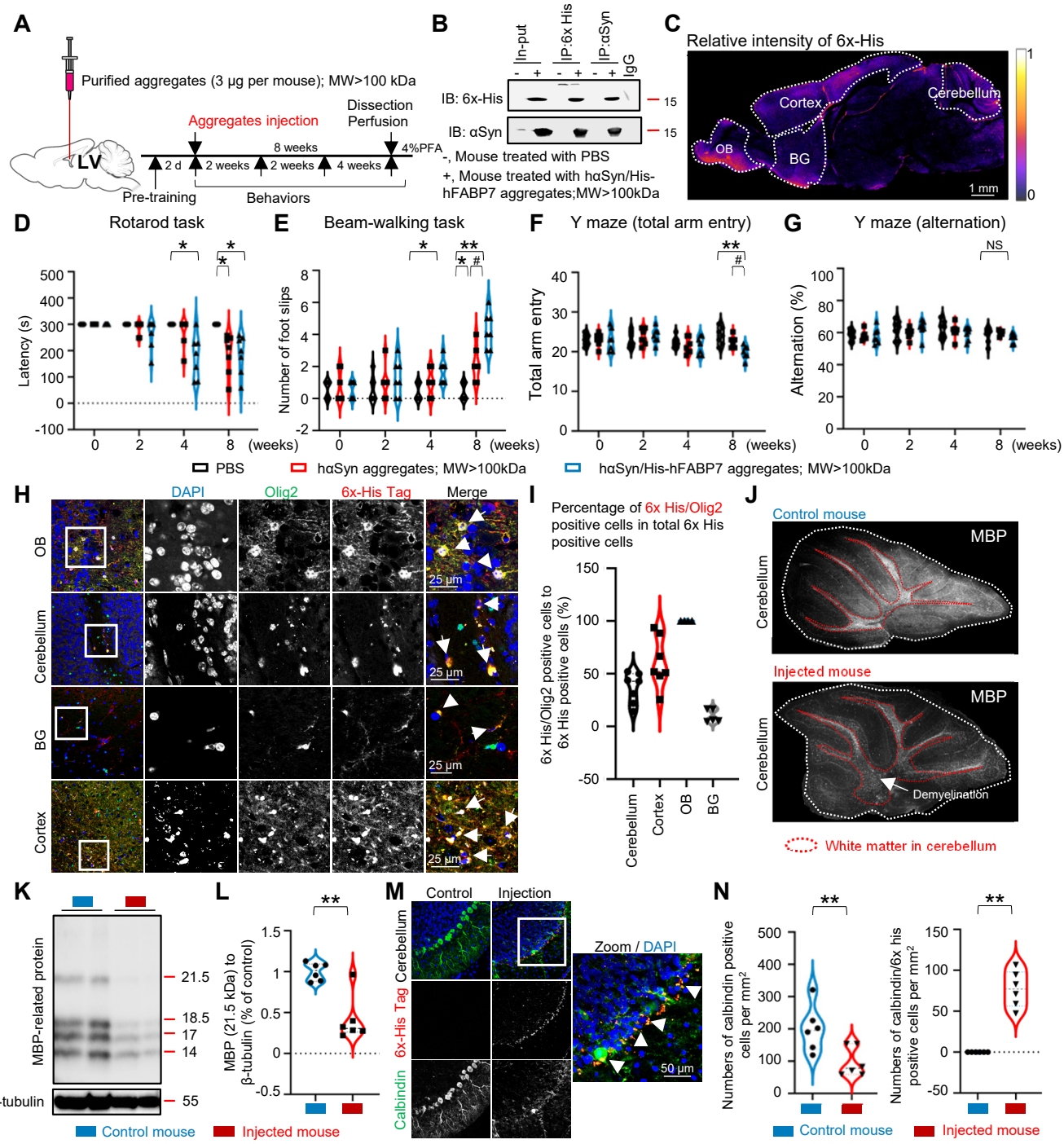

Unpublished Result

Figure 2

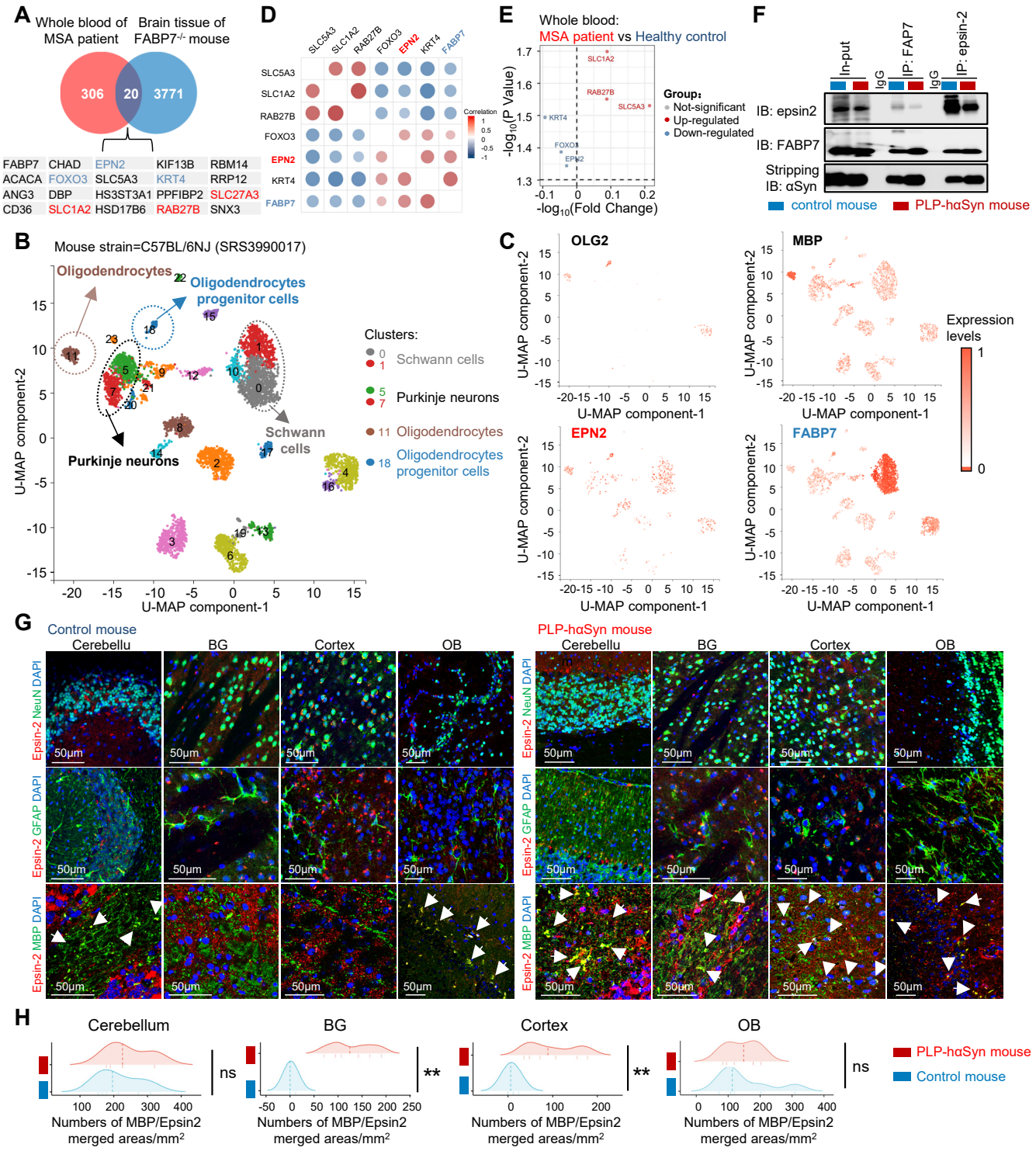
A
Whole blood of MSA patient
Brain tissue of FABP7-/- mouse
306
20
3771
FABP7 CHAD EPN2 KIF13B RBM14
ACACA FOXO3 SLC5A3 KRT4 RRP12
ANG3 DBP HS3ST3A1 PPFIBP2 SLC27A3
CD36 SLC1A2 HSD17B6 RAB27B SNX3
D
SLC5A3 SLC1A2 RAB27B FOXO3 EPN2 KRT4 FABP7
Correlation
E
Whole blood:
MSA patient vs Healthy control
-log10(P Value)
-log10(Fold Change)
Group:
Not-significant
Up-regulated
Down-regulated
F
In-put
IgG
IP: FAP7
IgG
IP: epsin-2
IB: epsin2
IB: FABP7
Stripping
IB: αSyn
control mouse
PLP-hαSyn mouse
B
Mouse strain=C57BL/6NJ (SRS3990017)
Oligodendrocytes
Oligodendrocytes progenitor cells
Purkinje neurons
Schwann cells
Clusters:
0 1 Schwann cells
5 7 Purkinje neurons
11 Oligodendrocytes
18 Oligodendrocytes progenitor cells
U-MAP component-1
U-MAP component-2
C
OLG2
MBP
EPN2
FABP7
Expression levels
G
Control mouse
PLP-hαSyn mouse
Cerebellu
BG
Cortex
OB
Epsin-2 NeuN DAPI
Epsin-2 GFAP DAPI
Epsin-2 MBP DAPI
50μm
H
Cerebellum
BG
Cortex
OB
ns
**
**
ns
Numbers of MBP/Epsin2 merged areas/mm2
PLP-hαSyn mouse
Control mouse

Figure 3

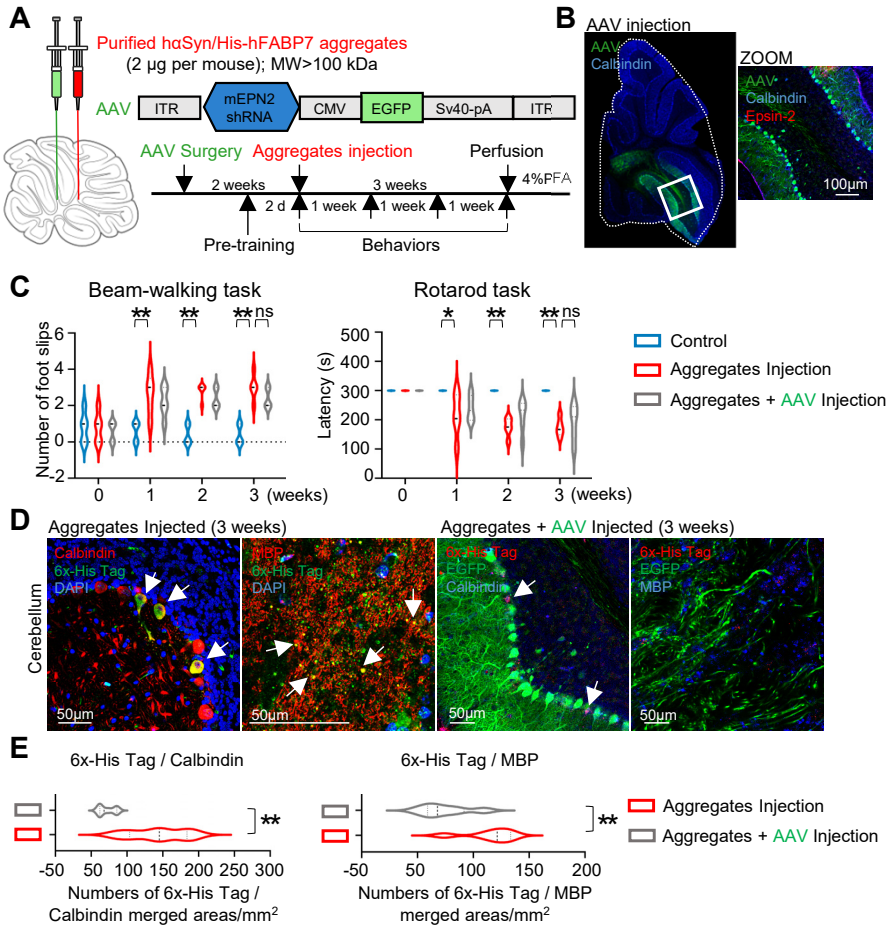
A
Purified hαSyn/His-hFABP7 aggregates
(2 μg per mouse); MW>100 kDa
AAV
ITR
mEPN2 shRNA
CMV
EGFP
Sv40-pA
ITR
AAV Surgery
Aggregates injection
Perfusion
2 weeks
3 weeks
4%PFA
2 d
1 week
1 week
1 week
Pre-training
Behaviors
B
AAV injection
AAV
Calbindin
ZOOM
AAV
Calbindin
Epsin-2
100μm
C
Beam-walking task
Rotarod task
Number of foot slips
Latency (s)
(weeks)
Control
Aggregates Injection
Aggregates + AAV Injection
D
Aggregates Injected (3 weeks)
Aggregates + AAV Injected (3 weeks)
Cerebellum
Calbindin
6x-His Tag
DAPI
MBP
EGFP
50μm
E
6x-His Tag / Calbindin
6x-His Tag / MBP
Numbers of 6x-His Tag / Calbindin merged areas/mm2
Numbers of 6x-His Tag / MBP merged areas/mm2
Aggregates Injection
Aggregates + AAV Injection

Figure 4

Supplementary Materials

Caption

1. Supplementary Figures (page 3-8)
2. Supplementary Tables (page 9-15)
3. Full-size scans of western blots (page 16)

Figures S1

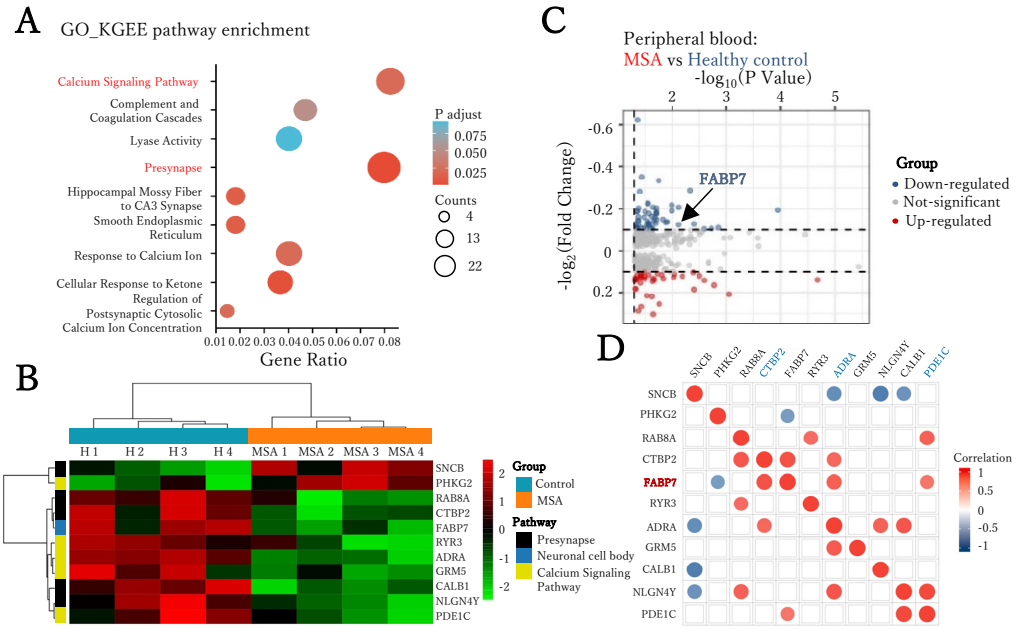

Figure S1. Related genes in MSA pathology. (A) GO analysis of pathways enriched for the genes that are more differentially expressed in the peripheral blood of MSA patient. (B) Heat map of normalized expression for 8 selected genes between healthy control and MSA patient. The color scale of the heat map indicated fold changes of expression for each gene: red, upregulated; green, downregulated. (C) Volcano plot of the log2 fold change (n=3) on the X-axis and log10 of the p-value derived using two-way ANOVA. Each point represents an individual mRNA; colored points represent significantly changed mRNA, and grey points represent non-significant mRNA. FABP7 is significantly ($p < 0.05$ and $|\log2\ FC| \geq 0.01$) downregulated in the peripheral blood of MSA patient. (D) Iteratively corrected map of selected genes, revealing three specific interactions, marked with Star symbol.

Figures S2

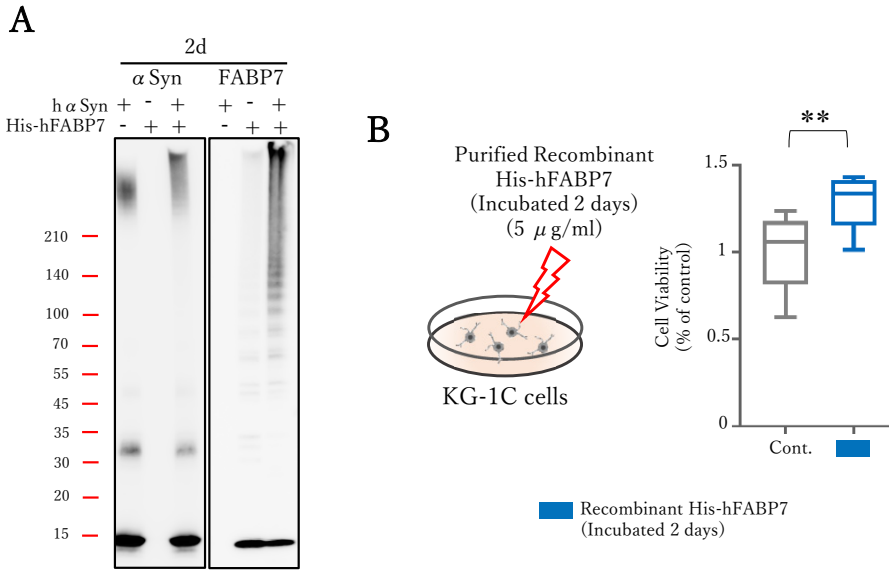

Figure S2. Recombinant His-hFABP7 suggests no obvious toxicity towards oligodendrocytes. A, Western blot analysis of α Syn and FABP7, human- α Syn and human-FABP7 were incubated in Tris-HCl (10 mM, pH=7.5) for two days. Incubation of His-hfabp7 only were not able to trigger high molecular weight aggregates. B, Cell viability analysis of KG-1C cells, based on a CCK assay. Cells cultured treated with separated fractions at a final concentrations of 5 μg/ml, for 24 h. The data are presented as the mean ± the standard error of the mean, were obtained using Unpaired Student`s t-test. **P < 0.01. α Syn, alpha-synuclein. CCK, cell counting kit-8; FABP7, fatty acid binding protein 7.

Figures S3

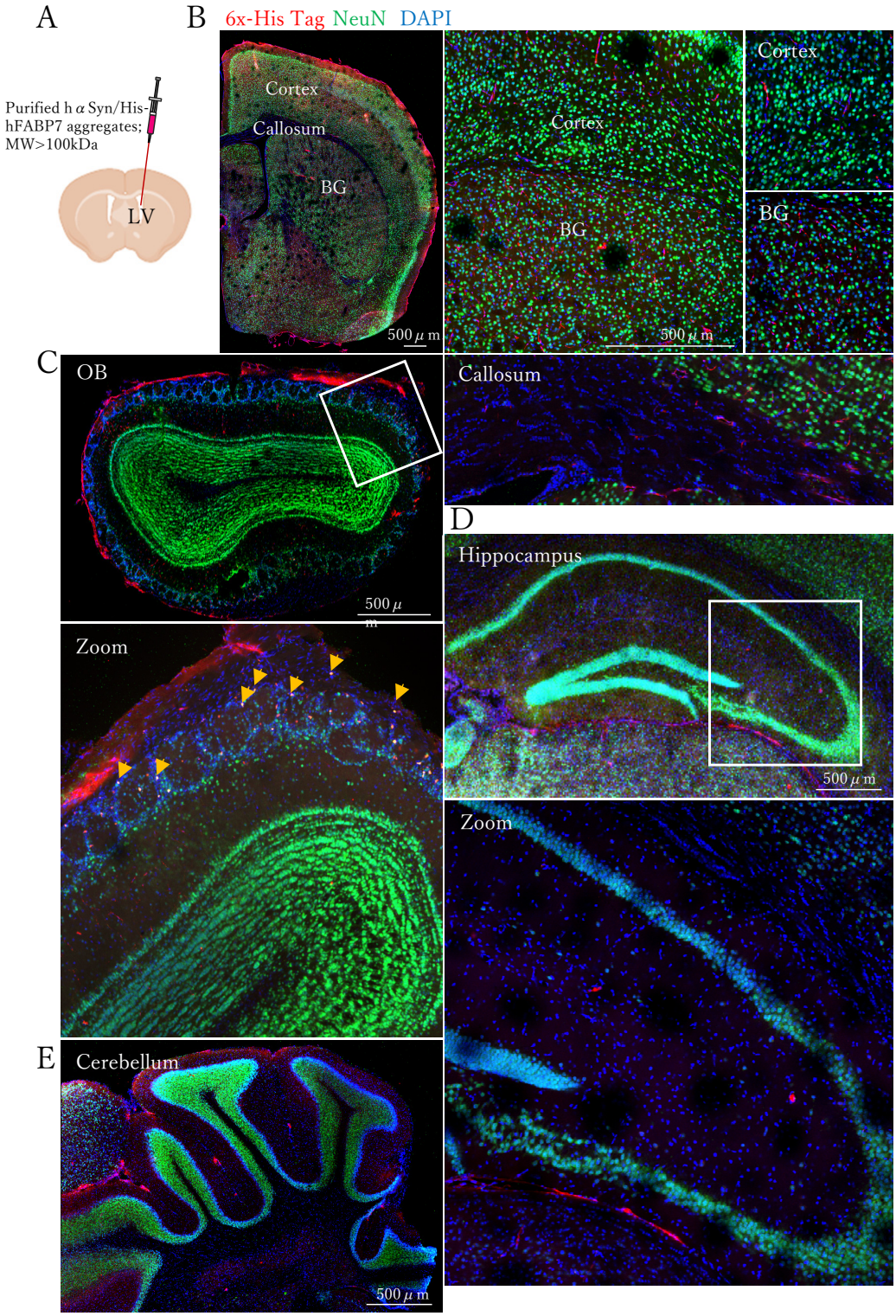

Figure S3. High molecular weight h α Syn/His-hFABP7 aggregates are not selectively taken up by neurons. A, Scheme of aggregates injection, α Syn/FABP7 aggregates were injected into Lateral Ventricles for 3 μ g per mouse. B, C, D, E, Confocal images show His-tagged aggregates in red, NeuN in green, DAPI in blue. h α Syn/His-hFABP7 aggregates are not selectively taken up by neurons in cortex, BG, hippocampus and cerebellum. But a small number of aggregates were taken up by neurons in OB. BG, basal ganglia; OB, olfactory bulb.

Figures S4

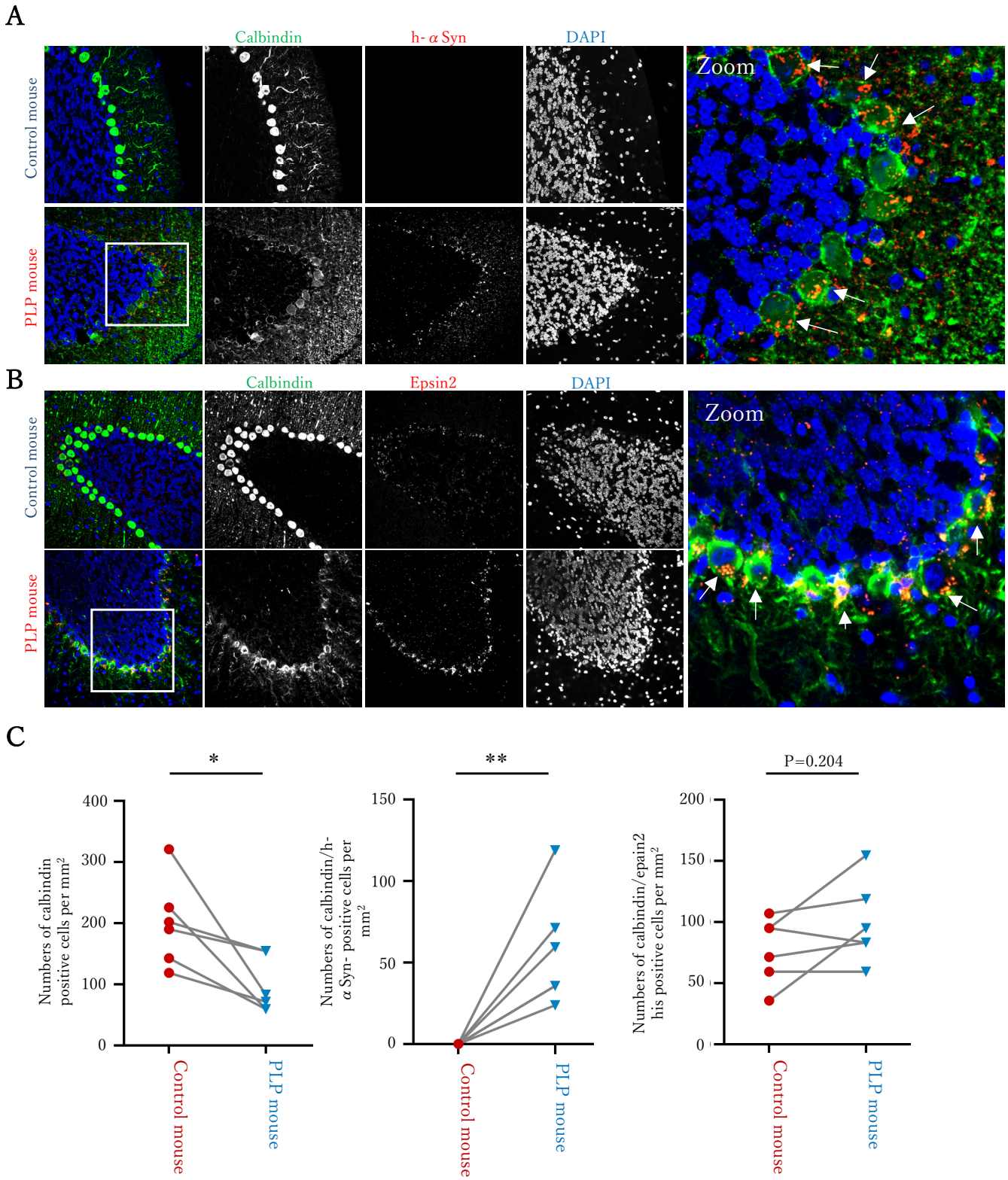

Figure S4. Purkinje cells also revealed MSA pathology association. A, Confocal images show h- α Syn in red, calbindin in green, DAPI in blue. h- α Syn localized in purkinje cells in PLP mouse. B, Confocal images show Epsin2 in red, calbindin in green, DAPI in blue. Epsin2 localized in purkinje cells in both Control and PLP mouse. C, Quantification of calbindin positive cells, of calbindin/h- α Syn- positive cells and calbindin/epain2 his positive cells. In PLP mouse the numbers of purkinje cells significantly decreased compared with control group and the calbindin/h- α Syn- positive cells increased significantly in PLP mouse. The data are presented as the mean ± the standard error of the mean, were obtained using Unpaired Student`s t-test. *P < 0.05 ; **P < 0.01. α Syn, alpha-synuclein.

Figures S5

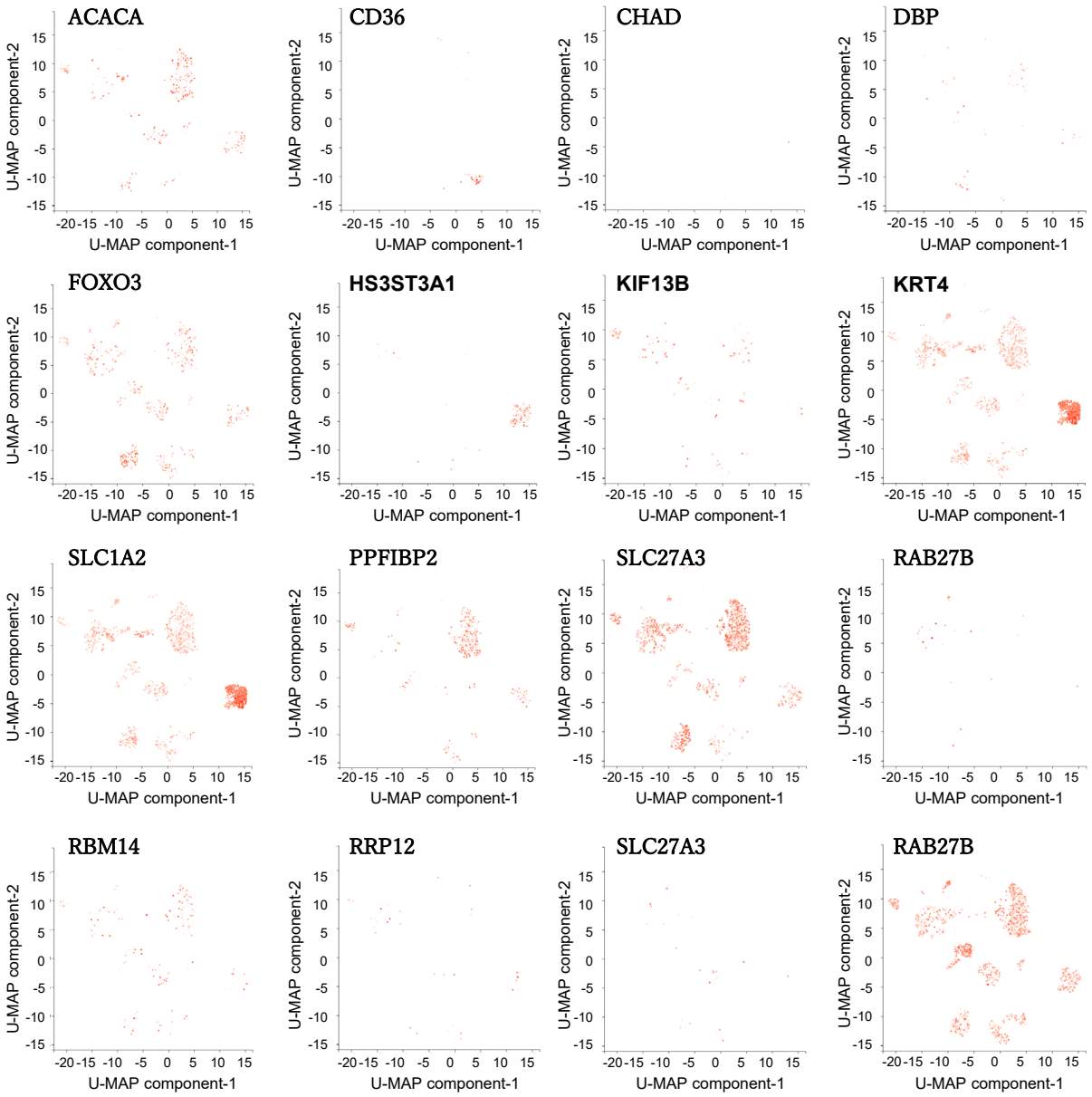

Figure S5. UMAP dimensional reduction visualizations of 5240 cells from olfactory bulb (mouse strain=C57BL/6NJ). Color represents normalized log expression of selected genes. Each point represents a cell. Original data were obtained from Gene Expression Omnibus (GEO; GSM3449587) and Sequencing data was handled using PanglaoDB (https://panglaodb.se/).

Figures S6

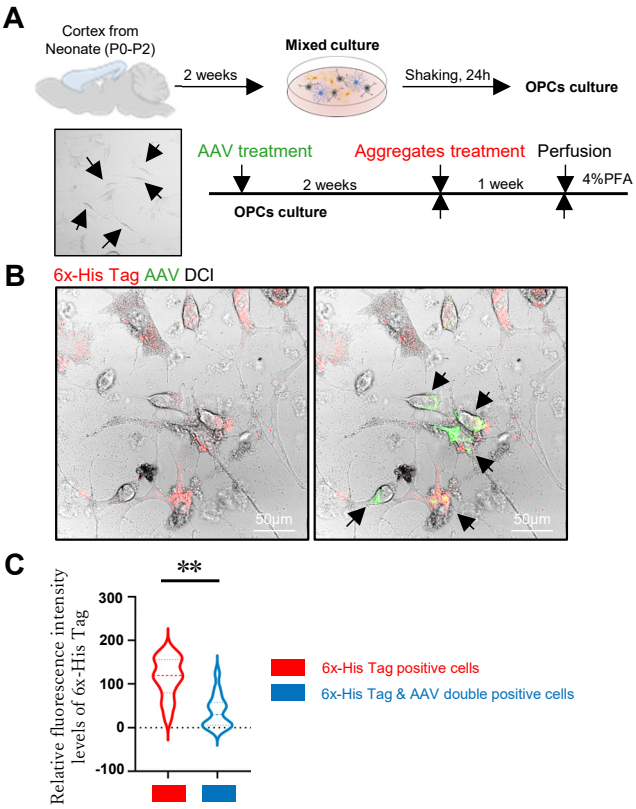

Figure S6. Downregulation of epsin2 decreased h α Syn/His-hFABP7 aggregates uptake in OPCs. A, Schematic diagram and treatment procedure of OPCs from the cortex of P1-2 mouse pups. B, Confocal images show aggregates in red, AAV in green. C, Quantification of B, suggested that the levels of h α Syn/His-hFABP7 aggregates uptake in OPCs decreased by epsin2 knock down. The data are presented as the mean ± the standard error of the mean, were obtained using Unpaired Student`s t-test. **$P < 0.01$. α Syn, alpha-synuclein.

Table S1; Raw data for Go and KEGG pathway analysis in Figure 1B

Category	Term	Count	%	PValue	Pop Hits	Pop Total	Fold Enrichment
KEGG	Olfactory transduction	120	4.28878	2.64E-08	1167	8977	1.628015578
KEGG	Pancreatic secretion	22	0.78628	7.29E-06	114	8977	3.055385377
KEGG	Salivary secretion	16	0.57184	2.40E-04	85	8977	2.980226165
KEGG	Yersinia infection	19	0.67906	0.00181	134	8977	2.244899839
KEGG	Neuroactive ligand-receptor interaction	37	1.32237	0.01135	386	8977	1.517618408
KEGG	Retrograde endocannabinoid signaling	18	0.64332	0.01169	148	8977	1.925568426
KEGG	Relaxin signaling pathway	16	0.57184	0.01554	129	8977	1.963714915
KEGG	Human cytomegalovirus infection	25	0.8935	0.03255	256	8977	1.546137842
KEGG	Spinocerebellar ataxia	16	0.57184	0.03195	141	8977	1.796590241
KEGG	Toll-like receptor signaling pathway	13	0.46462	0.02297	100	8977	2.058218695

Table S2; Raw data for Go and KEGG pathway analysis in Figure S1 A

ONTOLOGY	ID	Description	GeneRatio	BgRatio	pvalue	p.adjust	qvalue	Count
BP	GO:1901655	cellular response to ketone	10/273	93/18670	1.05337E-06	0.00400809	0.003550427	10
BP	GO:0051592	response to calcium ion	11/273	148/18670	1.16432E-05	0.020894972	0.018509081	11
BP	GO:0099566	regulation of postsynaptic cytosolic calcium ion concentration	4/273	12/18670	2.0184E-05	0.020894972	0.018509081	4
BP	GO:0019058	viral life cycle	16/273	328/18670	2.83649E-05	0.020894972	0.018509081	16
BP	GO:0008202	steroid metabolic process	16/273	331/18670	3.16645E-05	0.020894972	0.018509081	16
BP	GO:0006694	steroid biosynthetic process	12/273	196/18670	3.29487E-05	0.020894972	0.018509081	12
BP	GO:0050810	regulation of steroid biosynthetic process	8/273	95/18670	7.64179E-05	0.033739578	0.029887026	8
BP	GO:0019218	regulation of steroid metabolic process	9/273	124/18670	8.78035E-05	0.033739578	0.029887026	9
BP	GO:0031000	response to caffeine	4/273	17/18670	9.16034E-05	0.033739578	0.029887026	4
BP	GO:0036270	response to diuretic	4/273	17/18670	9.16034E-05	0.033739578	0.029887026	4
BP	GO:0010038	response to metal ion	16/273	364/18670	9.75389E-05	0.033739578	0.029887026	16
BP	GO:1901654	response to ketone	11/273	193/18670	0.000132664	0.042065605	0.037262347	11
BP	GO:0016125	sterol metabolic process	10/273	166/18670	0.000170314	0.047715001	0.042266666	10
BP	GO:1901653	cellular response to peptide	16/273	385/18670	0.000185515	0.047715001	0.042266666	16
BP	GO:1901617	organic hydroxy compound biosynthetic process	13/273	271/18670	0.000188101	0.047715001	0.042266666	13
BP	GO:0071277	cellular response to calcium ion	7/273	83/18670	0.000213087	0.050674704	0.044888416	7
BP	GO:0071384	cellular response to corticosteroid stimulus	6/273	61/18670	0.000261828	0.0586032	0.051911597	6
BP	GO:0006066	alcohol metabolic process	15/273	364/18670	0.000321295	0.063895342	0.056599456	15
BP	GO:0097306	cellular response to alcohol	7/273	89/18670	0.000328313	0.063895342	0.056599456	7
BP	GO:0050808	synapse organization	16/273	408/18670	0.000354508	0.063895342	0.056599456	16
BP	GO:0060537	muscle tissue development	16/273	408/18670	0.000354508	0.063895342	0.056599456	16
BP	GO:0008203	cholesterol metabolic process	9/273	150/18670	0.000369434	0.063895342	0.056599456	9
BP	GO:0031667	response to nutrient levels	18/273	499/18670	0.000420364	0.067558575	0.059844403	18
BP	GO:0048511	rhythmic process	13/273	295/18670	0.000426125	0.067558575	0.059844403	13
BP	GO:1902652	secondary alcohol metabolic process	9/273	155/18670	0.000469661	0.071426884	0.063271009	9
BP	GO:0071827	plasma lipoprotein particle organization	5/273	45/18670	0.000488068	0.071426884	0.063271009	5
BP	GO:0042594	response to starvation	10/273	191/18670	0.000522839	0.072554893	0.064270217	10
BP	GO:0035902	response to immobilization stress	4/273	27/18670	0.000602077	0.072554893	0.064270217	4
BP	GO:0034372	very-low-density lipoprotein particle remodeling	3/273	12/18670	0.000616945	0.072554893	0.064270217	3
BP	GO:0014706	striated muscle tissue development	15/273	390/18670	0.000658616	0.072554893	0.064270217	15
BP	GO:0007528	neuromuscular junction development	5/273	48/18670	0.000660083	0.072554893	0.064270217	5
BP	GO:0097305	response to alcohol	11/273	233/18670	0.000664226	0.072554893	0.064270217	11
BP	GO:0030301	cholesterol transport	7/273	100/18670	0.000665801	0.072554893	0.064270217	7
BP	GO:0046890	regulation of lipid biosynthetic process	10/273	198/18670	0.000691543	0.072554893	0.064270217	10
BP	GO:0034368	protein-lipid complex remodeling	4/273	28/18670	0.00069441	0.072554893	0.064270217	4
BP	GO:0034369	plasma lipoprotein particle remodeling	4/273	28/18670	0.00069441	0.072554893	0.064270217	4
BP	GO:0071825	protein-lipid complex subunit organization	5/273	49/18670	0.000726418	0.072554893	0.064270217	5
BP	GO:0019932	second-messenger-mediated signaling	16/273	439/18670	0.000781614	0.072554893	0.064270217	16
BP	GO:0034367	protein-containing complex remodeling	4/273	29/18670	0.000796331	0.072554893	0.064270217	4
BP	GO:0045540	regulation of cholesterol biosynthetic process	5/273	50/18670	0.00079761	0.072554893	0.064270217	5
BP	GO:0106118	regulation of sterol biosynthetic process	5/273	50/18670	0.00079761	0.072554893	0.064270217	5
BP	GO:0006695	cholesterol biosynthetic process	6/273	75/18670	0.000800869	0.072554893	0.064270217	6
BP	GO:1902653	secondary alcohol biosynthetic process	6/273	76/18670	0.000859026	0.076013792	0.067334162	6
BP	GO:0071375	cellular response to peptide hormone stimulus	13/273	321/18670	0.000934516	0.080814396	0.07158661	13
BP	GO:0050905	neuromuscular process	7/273	107/18670	0.000994861	0.082624912	0.073190391	7
BP	GO:0034370	triglyceride-rich lipoprotein particle remodeling	3/273	14/18670	0.000998882	0.082624912	0.073190391	3
BP	GO:0006006	glucose metabolic process	10/273	209/18670	0.001045654	0.082889861	0.073425087	10
BP	GO:0051701	interaction with host	10/273	209/18670	0.001045654	0.082889861	0.073425087	10
BP	GO:0016485	protein processing	13/273	328/18670	0.001136562	0.087738827	0.077720374	13
BP	GO:0071383	cellular response to steroid hormone stimulus	11/273	250/18670	0.001179593	0.087738827	0.077720374	11
BP	GO:0016126	sterol biosynthetic process	6/273	81/18670	0.001200203	0.087738827	0.077720374	6
BP	GO:0006390	mitochondrial transcription	3/273	15/18670	0.001235162	0.087738827	0.077720374	3
BP	GO:0034380	high-density lipoprotein particle assembly	3/273	15/18670	0.001235162	0.087738827	0.077720374	3
BP	GO:0062012	regulation of small molecule metabolic process	16/273	459/18670	0.001245177	0.087738827	0.077720374	16
BP	GO:0015918	sterol transport	7/273	112/18670	0.001299617	0.089909859	0.079643507	7
BP	GO:0017157	regulation of exocytosis	10/273	217/18670	0.00138691	0.091794595	0.081313035	10
BP	GO:0071241	cellular response to inorganic substance	10/273	217/18670	0.00138691	0.091794595	0.081313035	10
BP	GO:0035264	multicellular organism growth	8/273	146/18670	0.001399234	0.091794595	0.081313035	8
BP	GO:0043062	extracellular structure organization	15/273	422/18670	0.001450873	0.09229249	0.081754078	15
BP	GO:0070050	neuron cellular homeostasis	4/273	34/18670	0.00146838	0.09229249	0.081754078	4
BP	GO:0006957	complement activation, alternative pathway	3/273	16/18670	0.001503846	0.09229249	0.081754078	3
BP	GO:0071380	cellular response to prostaglandin E stimulus	3/273	16/18670	0.001503846	0.09229249	0.081754078	3
BP	GO:0071385	cellular response to glucocorticoid stimulus	5/273	58/18670	0.001568955	0.092963482	0.082348453	5
BP	GO:0014074	response to purine-containing compound	8/273	149/18670	0.001592455	0.092963482	0.082348453	8
BP	GO:0006631	fatty acid metabolic process	14/273	383/18670	0.001599168	0.092963482	0.082348453	14
BP	GO:0060291	long-term synaptic potentiation	6/273	86/18670	0.001636555	0.092963482	0.082348453	6
BP	GO:0071312	cellular response to alkaloid	4/273	35/18670	0.001638999	0.092963482	0.082348453	4
BP	GO:0010769	regulation of cell morphogenesis involved in differentiation	12/273	301/18670	0.001661371	0.092963482	0.082348453	12
BP	GO:0072330	monocarboxylic acid biosynthetic process	13/273	343/18670	0.001694218	0.093427533	0.082759516	13
BP	GO:0048167	regulation of synaptic plasticity	9/273	187/18670	0.001771149	0.096274587	0.08528148	9
BP	GO:0099509	regulation of presynaptic cytosolic calcium ion concentration	3/273	17/18670	0.00180647	0.096811501	0.085757086	3
BP	GO:0043470	regulation of carbohydrate catabolic process	6/273	88/18670	0.001841302	0.097307713	0.086196638	6
CC	GO:0098793	presynapse	22/276	491/19717	1.78085E-06	0.000808505	0.00068797	22
CC	GO:0005790	smooth endoplasmic reticulum	5/276	34/19717	0.000103434	0.012046609	0.01025065	5
CC	GO:0098686	hippocampal mossy fiber to CA3 synapse	5/276	34/19717	0.000103434	0.012046609	0.01025065	5
CC	GO:0098978	glutamatergic synapse	15/276	349/19717	0.000128574	0.012046609	0.01025065	15
CC	GO:0098984	neuron to neuron synapse	15/276	350/19717	0.000132672	0.012046609	0.01025065	15
CC	GO:0005924	cell-substrate adherens junction	16/276	408/19717	0.000219952	0.015912475	0.013540177	16
CC	GO:0030055	cell-substrate junction	16/276	412/19717	0.000245347	0.015912475	0.013540177	16
CC	GO:0030139	endocytic vesicle	13/276	303/19717	0.000365552	0.019015607	0.016180681	13
CC	GO:0044304	main axon	6/276	68/19717	0.000376961	0.019015607	0.016180681	6
CC	GO:0045335	phagocytic vesicle	8/276	132/19717	0.000549424	0.023612531	0.020092276	8
CC	GO:0098839	postsynaptic density membrane	6/276	74/19717	0.000594974	0.023612531	0.020092276	6
CC	GO:0005925	focal adhesion	15/276	405/19717	0.00062412	0.023612531	0.020092276	15
CC	GO:0014069	postsynaptic density	12/276	324/19717	0.002142323	0.066699813	0.056755927	12
CC	GO:0032279	asymmetric synapse	12/276	328/19717	0.002369628	0.066699813	0.056755927	12
CC	GO:0030666	endocytic vesicle membrane	8/276	167/19717	0.002487079	0.066699813	0.056755927	8
CC	GO:0043197	dendritic spine	8/276	169/19717	0.002676761	0.066699813	0.056755927	8
CC	GO:0044309	neuron spine	8/276	171/19717	0.002877567	0.066699813	0.056755927	8
CC	GO:0033267	axon part	13/276	382/19717	0.002967624	0.066699813	0.056755927	13
CC	GO:0099634	postsynaptic specialization membrane	6/276	101/19717	0.002976621	0.066699813	0.056755927	6
CC	GO:0030496	midbody	8/276	173/19717	0.003089935	0.066699813	0.056755927	8
CC	GO:0048786	presynaptic active zone	5/276	71/19717	0.003179591	0.066699813	0.056755927	5
CC	GO:0097060	synaptic membrane	14/276	432/19717	0.00323215	0.066699813	0.056755927	14
CC	GO:0099056	integral component of presynaptic membrane	5/276	73/19717	0.003586296	0.070790362	0.06023664	5
CC	GO:0099572	postsynaptic specialization	12/276	348/19717	0.00382049	0.072270934	0.061496482	12
CC	GO:0005788	endoplasmic reticulum lumen	11/276	309/19717	0.004359334	0.079064012	0.06727682	11
CC	GO:0043025	neuronal cell body	15/276	497/19717	0.004527895	0.079064012	0.06727682	15
CC	GO:0030176	integral component of endoplasmic reticulum membrane	7/276	150/19717	0.005260885	0.085301488	0.072584387	7
CC	GO:0098862	cluster of actin-based cell projections	7/276	150/19717	0.005260885	0.085301488	0.072584387	7
CC	GO:0034364	high-density lipoprotein particle	3/276	26/19717	0.005559011	0.08702728	0.074052891	3
CC	GO:0098889	intrinsic component of presynaptic membrane	5/276	82/19717	0.005887048	0.088400498	0.075221383	5
CC	GO:0045211	postsynaptic membrane	11/276	323/19717	0.006036157	0.088400498	0.075221383	11
CC	GO:0005791	rough endoplasmic reticulum	5/276	85/19717	0.006842712	0.095524145	0.081283008	5
CC	GO:0031227	intrinsic component of endoplasmic reticulum membrane	7/276	158/19717	0.006943385	0.095524145	0.081283008	7
CC	GO:0032154	cleavage furrow	4/276	55/19717	0.007322117	0.097771804	0.083195576	4
CC	GO:0042734	presynaptic membrane	7/276	161/19717	0.007667376	0.099456821	0.084629384	7
MF	GO:0016829	lyase activity	11/273	187/17697	0.000159465	0.09264909	0.08762175	11
KEGG	hsa04020	Calcium signaling pathway	14/170	201/8076	8.16215E-05	0.020731856	0.019846907	14
KEGG	hsa04610	Complement and coagulation cascades	8/170	85/8076	0.000396451	0.050349259	0.048200078	8

Table S3; Raw data for Gene expression of related pathway in Figure S1 B

ID	Healthy 1	Healthy 2	Healthy 3	Healthy 4	MSA 1	MSA 2	MSA 3	MSA 4
CALB1	2.955694	2.932365	2.978566	3.00914	2.865209	2.808293	2.840812	2.865586
SNCB	2.747565	2.815394	2.780871	2.719561	2.821542	2.917685	2.928274	2.894331
NLGN4Y	2.467353	2.355652	2.429973	2.387152	2.305952	2.332914	2.287684	2.254307
RAB8A	2.668973	2.59775	2.564751	2.590127	2.368003	2.551043	2.445178	2.431365
CTBP2	3.04549	3.021658	2.765157	2.923558	2.549863	2.706376	2.709497	2.721263
ADRA1D	3.645279	3.601824	3.575651	3.496773	3.193306	3.137624	3.171816	3.015327
GRM5	2.843392	2.858987	2.785304	2.718159	2.737629	2.682292	2.660426	2.67418
PHKG2	2.456556	2.397316	2.421394	2.377957	2.498782	2.444163	2.512519	2.478588
RYR3	2.797779	2.811571	2.806567	2.782739	2.762503	2.788361	2.729895	2.732739
PDE1C	2.770604	2.658156	2.695869	2.722476	2.634596	2.665939	2.606605	2.580159
FABP7	2.995158	3.024286	2.799255	3.018548	2.676231	2.745134	2.786901	2.649959

Table S4; Extended Data

Figure 1 I (left)			
Statistical analysis		**F (DFn, DFd)**	**P value**
One-way ANOVA with Tukey`s multiple comparisons test		F (2, 15)=8.055	P=0.0042
Comparison	**q**	**DF**	**P value**
Control vs h α Syn aggregates; MW<100kDa	1.572	15	0.522
Control vs h α Syn/His-hFABP7 aggregates; MW<100kDa	3.938	15	0.035
h α Syn aggregates; MW<100kDa vs h α Syn/His-hFABP7 aggregates; MW<100kDa	5.509	15	0.0039
Figure 1 I (right)			
Statistical analysis		**F (DFn, DFd)**	**P value**
One-way ANOVA with Tukey`s multiple comparisons test		F (2, 15)=18.31	P＜0.0001
Comparison	**q**	**DF**	**P value**
Control vs h α Syn aggregates; MW＞100kDa	4.611	15	0.0137
Control vs h α Syn/His-hFABP7 aggregates; MW＞100kDa	8.549	15	<0.0001
h α Syn aggregates; MW＞100kDa vs h α Syn/His-hFABP7 aggregates; MW＞100kDa	3.937	15	0.035
Figure 2 D			
Statistical analysis	**Interaction**	**F(DFn, DFd)**	**P value**
Two-way ANOVA withTukey`s multiple comparisons test	Row Factor	F (1.720, 10.32) = 7.869	P=0.0101
	Column Factor	F (1.373, 8.240) = 27.46	P=0.0004
	Row Factor x Column Factor	F (2.128, 12.77) = 4.798	P=0.0264
Comparison	0 weeks		
	q	**DF**	**P value**
Control vs h α Syn aggregates; MW＞100kDa	1.252	6	0.6682
Control vs h α Syn/His-hFABP7 aggregates; MW＞100kDa	0.2048	6	0.9885
h α Syn aggregates; MW＞100kDa vs h α Syn/His-hFABP7 aggregates; MW＞100kDa	2.187	6	0.3367
	2 weeks		
Control vs h α Syn aggregates; MW＞100kDa	1.453	6	0.5882
Control vs h α Syn/His-hFABP7 aggregates; MW＞100kDa	2.233	6	0.324
h α Syn aggregates; MW＞100kDa vs h α Syn/His-hFABP7 aggregates; MW＞100kDa	1.159	6	0.7056
	4 weeks		
Control vs h α Syn aggregates; MW＞100kDa	1.993	6	0.3945
Control vs h α Syn/His-hFABP7 aggregates; MW＞100kDa	5.587	6	0.0177
h α Syn aggregates; MW＞100kDa vs h α Syn/His-hFABP7 aggregates; MW＞100kDa	3.069	6	0.1555
	8 weeks		
Control vs h α Syn aggregates; MW＞100kDa	5.572	6	0.0179
Control vs h α Syn/His-hFABP7 aggregates; MW＞100kDa	5.795	6	0.015
h α Syn aggregates; MW＞100kDa vs h α Syn/His-hFABP7 aggregates; MW＞100kDa	0.6513	6	0.8917

Figure 2 E			
Statistical analysis	**Interaction**	**F(DFn, DFd)**	**P value**
Two-way ANOVA with Tukey`s multiple comparisons test	Row Factor	F (1.916, 11.50) = 14.71	P=0.0007
	Column Factor	F (1.459, 8.752) = 32.90	P=0.0002
	Row Factor x Column Factor	F (3.244, 19.46) = 6.781	P=0.0022
Comparison		0 weeks	
	q	**DF**	**P value**
Control vs h α Syn aggregates; MW > 100kDa	0.5941	6	0.9087
Control vs h α Syn/His-hFABP7 aggregates; MW > 100kDa			
h α Syn aggregates; MW > 100kDa vs h α Syn/His-hFABP7 aggregates; MW > 100kDa	0.5941	6	0.9087
		2 weeks	
Control vs h α Syn aggregates; MW > 100kDa	1.148	6	0.7102
Control vs h α Syn/His-hFABP7 aggregates; MW > 100kDa	1.786	6	0.4634
h α Syn aggregates; MW > 100kDa vs h α Syn/His-hFABP7 aggregates; MW > 100kDa	1.124	6	0.7197
		4 weeks	
Control vs h α Syn aggregates; MW > 100kDa	2.191	6	0.3356
Control vs h α Syn/His-hFABP7 aggregates; MW > 100kDa	5.058	6	0.0272
h α Syn aggregates; MW > 100kDa vs h α Syn/His-hFABP7 aggregates; MW > 100kDa	1.936	6	0.4126
		8 weeks	
Control vs h α Syn aggregates; MW > 100kDa	4.648	6	0.0383
Control vs h α Syn/His-hFABP7 aggregates; MW > 100kDa	11.88	6	0.0004
h α Syn aggregates; MW > 100kDa vs h α Syn/His-hFABP7 aggregates; MW > 100kDa	5.477	6	0.0193

Figure 2 F			
Statistical analysis	**Interaction**	**F(DFn, DFd)**	**P value**
Two-way ANOVA withTukey`s multiple comparisons test	Row Factor	F (6, 72) = 2.469	P=0.0315
	Column Factor	F (3, 72) = 3.600	P=0.0175
	Row Factor x Column Factor	F (2, 72) = 2.053	P=0.1358
Comparison		0 weeks	
	q	**DF**	**P value**
Control vs h α Syn aggregates; MW > 100kDa	0	72	>0.9999
Control vs h α Syn/His-hFABP7 aggregates; MW > 100kDa	0.1966	72	0.9894
h α Syn aggregates; MW > 100kDa vs h α Syn/His-hFABP7 aggregates; MW > 100kDa	0.1966	72	0.9894
		2 weeks	
Control vs h α Syn aggregates; MW > 100kDa	0.9832	72	0.767
Control vs h α Syn/His-hFABP7 aggregates; MW > 100kDa	1.376	72	0.596
h α Syn aggregates; MW > 100kDa vs h α Syn/His-hFABP7 aggregates; MW > 100kDa	0.3933	72	0.9583
		4 weeks	
Control vs h α Syn aggregates; MW > 100kDa	1.376	72	0.596
Control vs h α Syn/His-hFABP7 aggregates; MW > 100kDa	1.18	72	0.6831
h α Syn aggregates; MW > 100kDa vs h α Syn/His-hFABP7 aggregates; MW > 100kDa	0.1966	72	0.9894
		8 weeks	
Control vs h α Syn aggregates; MW > 100kDa	1.966	72	0.3512
Control vs h α Syn/His-hFABP7 aggregates; MW > 100kDa	5.703	72	0.0004
h α Syn aggregates; MW > 100kDa vs h α Syn/His-hFABP7 aggregates; MW > 100kDa	3.736	72	0.027

Figure 2 G			
Statistical analysis	**Interaction**	**F(DFn, DFd)**	**P value**
Two-way ANOVA withTukey`s multiple comparisons test	Row Factor	F (6, 72) = 0.8689	P=0.5221
	Column Factor	F (3, 72) = 3.589	P=0.0177
	Row Factor x Column Factor	F (2, 72) = 0.5345	P=0.5883
Comparison		0 weeks	
	q	**DF**	**P value**
Control vs h α Syn aggregates; MW > 100kDa	0.1792	72	0.9912
Control vs h α Syn/His-hFABP7 aggregates; MW > 100kDa	0.1971	72	0.9893
h α Syn aggregates; MW > 100kDa vs h α Syn/His-hFABP7 aggregates; MW > 100kDa	0.01792	72	>0.9999
		2 weeks	
Control vs h α Syn aggregates; MW > 100kDa	1.416	72	0.5785
Control vs h α Syn/His-hFABP7 aggregates; MW > 100kDa	0.5198	72	0.9283
h α Syn aggregates; MW > 100kDa vs h α Syn/His-hFABP7 aggregates; MW > 100kDa	1.936	72	0.3626
		4 weeks	
Control vs h α Syn aggregates; MW > 100kDa	0.8065	72	0.8363
Control vs h α Syn/His-hFABP7 aggregates; MW > 100kDa	1.819	72	0.4075
h α Syn aggregates; MW > 100kDa vs h α Syn/His-hFABP7 aggregates; MW > 100kDa	1.013	72	0.7548
		8 weeks	
Control vs h α Syn aggregates; MW > 100kDa	0.8244	72	0.8297
Control vs h α Syn/His-hFABP7 aggregates; MW > 100kDa	1.425	72	0.5746
h α Syn aggregates; MW > 100kDa vs h α Syn/His-hFABP7 aggregates; MW > 100kDa	2.249	72	0.2563

Figure 2 L			
Statistical analysis	**Unpaired Student`s t-test**		
Comparison	**t**	**DF**	**P value**
Control mouse vs Injected mouse	4.817	10	0.0007
Figure 2 N (left)			
Statistical analysis	**Unpaired Student`s t-test**		
Comparison	**t**	**DF**	**P value**
Control mouse vs Injected mouse	2.992	10	0.0135
Figure 2 L (right)			
Statistical analysis	**Unpaired Student`s t-test**		
Comparison	**t**	**DF**	**P value**
Control mouse vs Injected mouse	8.51	10	<0.0001
Figure 3 H (Cerebellum)			
Statistical analysis	**Unpaired Student`s t-test**		
Comparison	**t**	**DF**	**P value**
Control mouse vs PLP mouse	0.766	10	0.4613
Figure 3 H (Cortex)			
Statistical analysis	**Unpaired Student`s t-test**		
Comparison	**t**	**DF**	**P value**
Control mouse vs PLP mouse	6.807	10	<0.0001
Figure 3 H (BG)			
Statistical analysis	**Unpaired Student`s t-test**		
Comparison	**t**	**DF**	**P value**
Control mouse vs PLP mouse	3.791	10	0.0035
Figure 3 H (OB)			
Statistical analysis	**Unpaired Student`s t-test**		
Comparison	**t**	**DF**	**P value**
Control mouse vs PLP mouse	0.2396	10	0.8155
Figure 4 C (Beam-walking)			
Statistical analysis	**Interaction**	**F(DFn, DFd)**	**P value**
Two-way ANOVA withTukey`s multiple comparisons test	Row Factor x Time	F (6, 32) = 4.560	P=0.0019
	Row Factor	F (3, 16) = 8.974	P=0.0010
	Time	F (2, 32) = 36.04	<0.0001
Comparison	0 weeks		
	t	**DF**	**P value**
Control vs aggregates injection	0	32	>0.9999
Control vs aggregates+AAV injection	0.4629	32	>0.9999
aggregates injection vs aggregates+AAV injection	0.4629	32	>0.9999
	1 weeks		
Control vs aggregates injection	4.629	32	0.0007
Control vs aggregates+AAV injection	3.703	32	0.0096
aggregates injection vs aggregates+AAV injection	0.9258	32	0.9954
	2 weeks		
Control vs aggregates injection	5.555	32	<0.0001
Control vs aggregates+AAV injection	4.629	32	0.0007
aggregates injection vs aggregates+AAV injection	0.9258	32	0.9954
	3 weeks		
Control vs h α Syn aggregates; MW＞100kDa	6.018	32	<0.0001
Control vs h α Syn/His-hFABP7 aggregates; MW＞100kDa	4.629	32	0.0007
h α Syn aggregates; MW＞100kDa vs h α Syn/His-hFABP7 aggregates; MW＞100kDa	1.389	32	0.8999

Figure 4 C (Rotarod)			
Statistical analysis	**Interaction**	**F(DFn, DFd)**	**P value**
Two-way ANOVA withTukey`s multiple comparisons test	Row Factor x Time	F (6, 32) = 3.281	P=0.0125
	Row Factor	F (3, 16) = 14.92	P<0.0001
	Time	F (2, 32) = 25.39	P<0.0001
Comparison	0 weeks		
	t	**DF**	**P value**
Control vs aggregates injection	0	32	>0.9999
Control vs aggregates+AAV injection	0	32	>0.9999
aggregates injection vs aggregates+AAV injection	0	32	>0.9999
	1 weeks		
Control vs aggregates injection	3.415	32	0.0208
Control vs aggregates+AAV injection	2.458	32	0.2112
aggregates injection vs aggregates+AAV injection	0.9572	32	0.9938
	2 weeks		
Control vs aggregates injection	5.086	32	0.0002
Control vs aggregates+AAV injection	3.626	32	0.0118
aggregates injection vs aggregates+AAV injection	1.46	32	0.8656
	3 weeks		
Control vs h α Syn aggregates; MW＞100kDa	5.094	32	0.0002
Control vs h α Syn/His-hFABP7 aggregates; MW＞100kDa	4.421	32	0.0013
h α Syn aggregates; MW＞100kDa vs h α Syn/His-hFABP7 aggregates; MW＞100kDa	0.6733	32	0.9998

Figure 4 E (left)			
Statistical analysis	Unpaired Student`s t-test		
Comparison	**t**	**DF**	**P value**
Aggregates Injection mouse vs Aggregates + AAV Injection mouse	4.119	10	0.0021

Figure 4 E (right)			
Statistical analysis	Unpaired Student`s t-test		
Comparison	**t**	**DF**	**P value**
Aggregates Injection mouse vs Aggregates + AAV Injection mouse	3.312	10	0.0079

Figure S2 B (left)			
Statistical analysis	Unpaired Student`s t-test		
Comparison	**t**	**DF**	**P value**
Control mouse vs PLP mouse	3.154	14	0.007

Full-size scans of western blots

Figure1 C

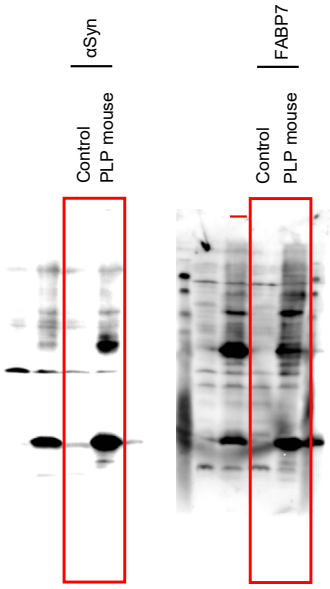

Figure1 F

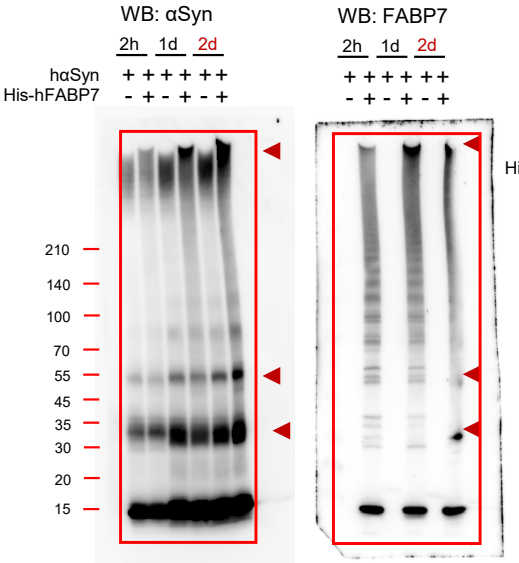

Figure1 H

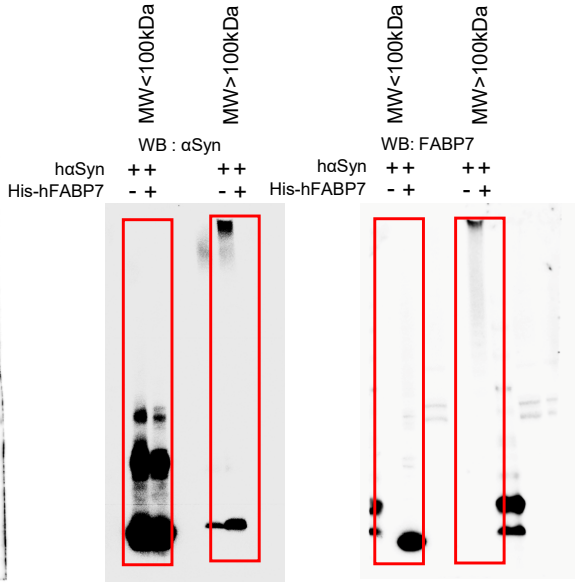

Figures S2

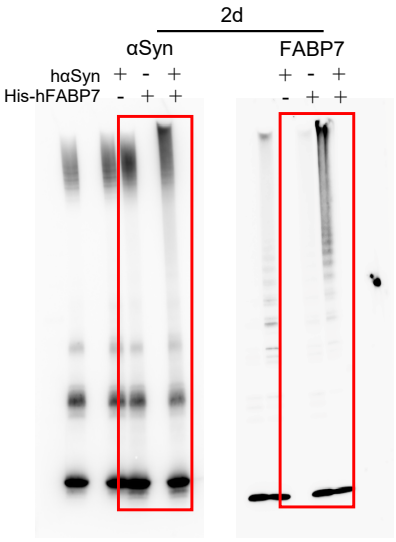

Figure2 B

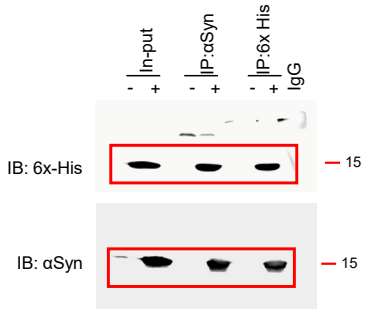

Figure2 K

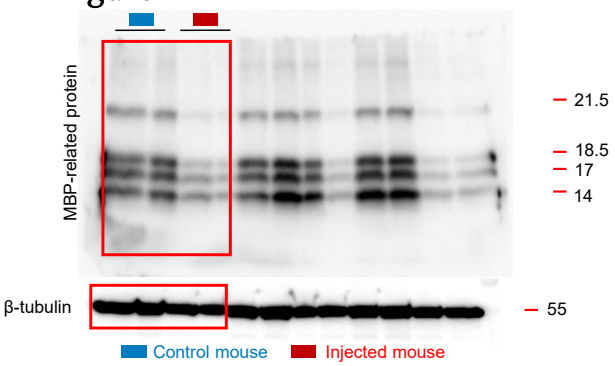
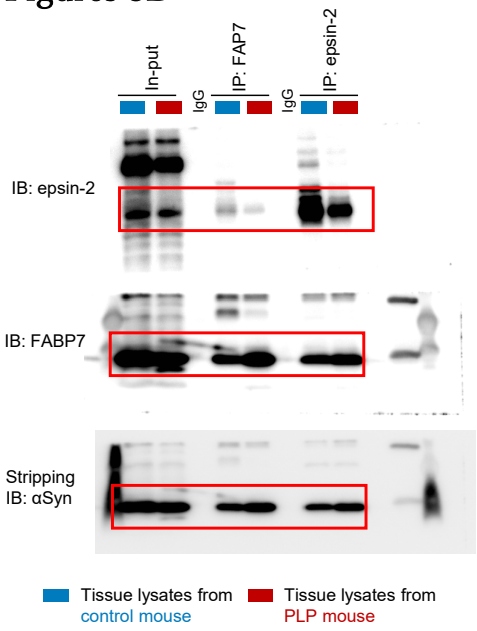
Figures 3D